Strange metal in the doped Hubbard model via percolation

Andrew A. Allocca*
Department of Physics and Astronomy and Center for Computation and Technology, Louisiana State University, Baton Rouge, LA 70803, USA

Many strongly correlated systems, including high-temperature superconductors such as the cuprates, exhibit strange metallic behavior in certain parameter regimes characterized by anomalous transport properties that are irreconcilable with a Fermi-liquid-like description in terms of quasiparticles. The Hubbard model is a standard theoretical starting point to examine the properties of such systems and also exhibits non-Fermi-liquid behavior in simulations. Here we analytically study the two-dimensional hole-doped Hubbard model, first identifying a percolation transition that occurs in the low-energy sector at critical hole doping $p_c \sim 0.19$. We then use the critical properties near this transition to rewrite the Hubbard Hamiltonian in a way that motivates a large-N model with strange metallic properties. In particular, we show that this model has the linear-in-T resistivity and power-law optical conductivity $\sim |\omega|^{-2/3}$ observed in the strange metal regime of cuprates, suggesting potential relevance for describing this important class of materials.

I. INTRODUCTION

The strange metal phase of the hole-doped cuprate superconductors is characterized by a dc-resistivity with anomalous linear temperature dependence $\rho \sim T$ [1, 2] starkly different from the quadratic behavior in normal metals described by Fermi liquid theory. This behavior persists from the melting of low-temperature ordered phases up to very high temperatures with no significant change in slope and is seen over a range of doping levels p. It is most prominent near optimal doping or the critical value p_c signalling the collapse of the pseudogap phase, with a gradual crossover from $\rho \sim T$ around these values to more standard Fermi-liquid-like $\rho \sim T^2$ far enough into the overdoped regime [3–5]. Studies of other properties find additional anomalous, non-Fermi-liquid-like behaviors, such as power-law scaling of the optical conductivity $\sigma(\omega) \sim |\omega|^{-\gamma}$ over a finite frequency range, with $\gamma \approx 2/3$ at p_c [6–11] and a Hall angle obeying $\cot\Theta_H \sim AT^2 + B$ across a wide range of doping levels [12–14].

In addition to this phenomenology, there is growing experimental evidence for a temperature-independent phenomenon in the cuprates occurring at the critical hole doping p_c. Transport measurements in LSCO subjected to magnetic fields strong enough to suppress superconductivity find a broad range of dopings at low temperatures supporting T-linear resistivity [5], with features in the doping dependence of the resistivity at $p_c \approx 0.185$; the coefficients of T and T^2 terms fitting the measured behavior of ρ have distinct features at p_c, with the linear coefficient achieving its maximum value. As noted in Ref. [5], this phenomenology contrasts with the behavior expected from a quantum phase transition, which would produce this behavior in only a narrow fan emerging from the quantum critical point, not a broad region at low temperature. A more recent ARPES study of Bi2212 [15] identified a T-independent boundary in the temperature-doping phase diagram at $p_c \sim 0.19$ across which the spectral function near the Brillouin zone boundary abruptly changes from incoherent below p_c to coherent with an identifiable quasiparticle peak above p_c.

Evidence of non-Fermi liquid behavior is also found in studies of the Hubbard model on a two-dimensional square lattice, believed to model essential features of the CuO_2 planes of the cuprates as well as being the prototype for more general systems of strongly correlated electrons [16, 17]. Numerical analyses identify marginal Fermi-liquid [18] behavior of the electronic self-energy in hole-doped systems at nonzero temperature [19, 20], and show that linear-in-T resistivity persists down to low temperature [21, 22], connecting with studies finding T-linear behavior at high temperatures [23]. Simulations of the Hubbard model in systems of cold atoms also extract diffusion and transport properties that are consistent with linear-in-T charge transport [24, 25]. Thus, the Hubbard model is itself sufficient to produce the defining strange metal phenomenology $\rho \sim T$, and phenomena in real materials such as interactions with phonons, structural transitions, disorder, etc. are evidently not necessary ingredients to realize this behavior.

The T-linear nature of the resistivity and the other unusual properties in strange metals appear to be inconsistent with a description of these system in terms of quasiparticles. Current is dissipated on a time scale $\tau \sim \hbar/k_B T$ depending only on temperature, demonstrating that at least the charge-carrying sector of these systems contain no other characteristic energy scale, such as a quasiparticle mass. Consequently, in recent years there has been a great amount of theoretical work aiming to better understand strongly-interacting systems without quasiparticles, such as the Sachdev-Ye-Kitaev (SYK) model and its large-N relatives [26–34], or those with holographic dualities to gravitational theories [35]. Other approaches explore destroying the electronic Fermi surface via coupling to critical bosons [36–39], or invoke the intrinsically non-quasiparticle concept of unparticles [40–44]. Still other work takes a model-agnostic hydrody-

* aallocca@lsu.edu

namic approach to study systems with anomalous transport properties [45–49].

Taking experimental, numerical, and theoretic insights together, we propose that a model for the strange metal phase of the cuprates can in principle be obtained from the Hubbard Hamiltonian on a 2d square lattice without any additional effects such as phonons, disorder, or structural transitions, and without introducing additional degrees of freedom by hand. This model should be able to naturally reproduce generic experimental phenomena, such as T-independent features at $p_c \sim 0.19$, T-linear resistivity, power-law optical conductivity, and the appearance of coherent quasiparticles and crossover to Fermi liquid behavior for $p > p_c$. There is existing work examining non-Fermi-liquid phenomena in doped Mott insulators [28] which hits close to this aim, however there the system is composed of $SU(N)$ spins with an artificial large-N limit, following Ref. [26], instead of the physical case of spin-1/2.

Here we motivate a theory satisfying many of these criteria by working in a many-body basis for the large-U 2d Hubbard model that leverages the structure of a classical percolation transition [50] occurring in generic many-electron states. For a generic configuration of electrons in the lattice without doubly-occupied sites, electrons of one spin species bound clusters of sites that contain all electrons of the opposite spin. In such a generic state electron positions are random and uncorrelated, and a straightforward calculation shows a percolation transition in these clusters at a critical doping $p_c \approx 0.1854$ independent of temperature, very close to the value in the cuprates. For $p \sim p_c$ the properties of these clusters are thus dictated by a critical theory, and re-expressing the Hubbard Hamiltonian in terms of these clusters we find that the dynamics of the system can be expressed in terms of their shifting, merging, and dividing. We write an approximate large-N model from this Hamiltonian valid near the transition where the N "flavors" in this model are ultimately related to the large number of possible shapes of large clusters. Examining the transport properties of this model we find linear-in-T dc resistivity and a power-law contribution to the optical conductivity $\sigma(\omega) \sim |\omega|^{-2/3}$ for a range of frequencies, matching what is seen in experiments in the cuprates.

The remainder of this paper is organized as follows. In Section II we give a brief introduction to relevant aspects of site percolation and clusters, which will be used throughout the rest of the analysis. We start our analysis of the Hubbard model in Section III, introducing the cluster basis and cluster operators, and rewriting the Hubbard Hamiltonian in terms of these degrees of freedom. In Section IV we discuss approximations to this form of the Hamiltonian, which motivates the large-N model action we write and begin to analyze in Section V. In Section VI we calculate the anomalous transport properties of the model, and finally in Section VII we discuss these results and the outlook for further developments.

II. 2D SITE PERCOLATION

Since it is central to our construction and establishes notation used throughout, we begin with a brief summary of relevant aspects of percolation theory, as given in Refs. [50, 51]. In a site percolation model, the sites of an infinite lattice are randomly and independently occupied with some probability P, and the average properties of clusters of occupied sites are then analyzed as functions of P. Two occupied sites belong to the same cluster if they are nearest-neighbors, and the number of sites comprising a cluster, which we call its size, is denoted with s. Some quantities of interest are the size of the largest cluster, the average cluster size, and the distribution of cluster sizes. Importantly, a phase transition occurs in this system as the occupation probability passes through a critical value P_c. For $P < P_c$ the system has only finite clusters—average s is finite and the largest cluster has size s_ξ. As $P \to P_c$ from below s_ξ diverges, and for $P > P_c$ there is single infinite cluster which encompasses an ever larger portion of all sites in the system for increasing P. At $P = P_c$ the system has clusters of every finite size, no characteristic scale, and can be described by a conformal field theory. For the 2d square lattice, which is our primary interest, this critical occupation probability is $P_c \approx 0.5927$.

Near to the critical point the average properties and distribution of finite clusters obey a scaling theory controlled by $|P - P_c|$ and characterized by critical exponents. For $P < P_c$ the average number of sites in the largest finite cluster is $s_\xi \propto |P - P_c|^{-1/\sigma_P}$ and the average linear size of this cluster is the correlation length $\xi_P \propto |P - P_c|^{-\nu_P}$, with critical exponents $\sigma_P = 36/91$ and $\nu_P = 4/3$ in two dimensions [52]. The two are related through $s_\xi \propto \xi_P^{d_f}$, where $d_f = 1/(\nu_P \sigma_P) = 91/48$ is a fractal dimension characterizing the scaling between these quantities on average for large s. Motivated by this, for large enough s we can define an average cluster radius R through $s \propto R^{d_f}$. For large s the average density of clusters of size s is $n_s \propto s^{-\tau_P} f(s/s_\xi)$ with critical exponent $\tau_P = 187/91$, where the function f is constant for small argument and rapidly decays for argument greater than 1. The total density of clusters is the sum of n_s over all s, $M_0 = \sum_s n_s$, and the critical part of this density generated by large clusters is

$$M_{0,\text{crit}} \equiv \sum_s n_s \Big|_{\text{crit}} \propto |P - P_c|^{2-\alpha_P}, \tag{1}$$

where in 2d we have the critical exponent $\alpha_P = -2/3$.

These scaling relationships only apply for large enough clusters. Small clusters contribute analytic terms for some quantities, but are largely irrelevant for critical properties near the transition. We use s_0 to denote the cluster size above which these scaling properties hold, and $R_0 \gg a$ for the corresponding radius, where a is the lattice constant.

III. REWRITING THE HUBBARD HAMILTONIAN

Turning now to an electronic system, we write the Hubbard Hamiltonian in a square lattice with isotropic nearest neighbor hopping as

$$\begin{aligned} H &= H_U + H_\uparrow + H_\downarrow \\ H_U &= U \sum_i n_{i,\uparrow} n_{i,\downarrow} \\ H_\sigma &= -t \sum_{\langle ij \rangle} c^\dagger_{i,\sigma} c_{j,\sigma} - \mu_p \sum_i c^\dagger_{i,\sigma} c_{i,\sigma}, \end{aligned} \tag{2}$$

where U is the on-site Coulomb repulsion energy, taken to be the largest energy scale, t is the hopping energy, $n_{i,\sigma} = c^\dagger_{i,\sigma} c_{i,\sigma}$ is the number of spin-σ electrons on site i, and μ_p is a chemical potential, dependent on the doping p, that controls the total electron density. We consider only hole-doped systems with no net magnetization, so the number of electrons N_e is less than the number of lattice sites N and the numbers of spin-up and spin-down electrons are equal, $N_\uparrow = N_\downarrow = N_e/2$. The number of doped holes is $N_h = N - N_e$, so the hole doping is $p = N_h/N$, and similarly the electron density is $n_e = N_e/N$.

To build our model we consider the three terms of Eq. (2) in turn, and the full process is outlined schematically in Fig. 1. First, H_U restricts the set of real-space basis states that we are free to use—large on-site repulsion $U \gg t, T$, essentially forbids doubly-occupied sites, so for a hole-doped system each site contains either a single electron or is empty, $n_e + p = 1$ [53]. We can separate this Hilbert space into groups of states based on the positions of spin-down electrons; all states in a given group have spin-down electrons in the same positions, with only the positions of spin-up electrons differing between them. Thus, states in each group are related to each other by spin-up electron hopping within fixed, disjoints clusters of available sites. Indeed, the set of these clusters of sites is in exact one-to-one correspondence with the positions of the spin-down electrons forming their boundaries, and either acts as a good label for states.

Next, focusing in on the level of a single cluster, we transform from the position basis for spin-up electrons to the eigenbasis of the spin-up hopping Hamiltonian $H_\uparrow$ within each cluster. Instead of definite position, spin-up electrons occupy states of definite energy with weight spread over many sites in a cluster, and many-electron states are given by Slater determinants of the corresponding wave functions. We can write composite operators to create many-electron states in any cluster, and all basis states for the full system can be expressed in terms of these composite "cluster operators."

Finally, the remaining spin-down hopping term $H_\downarrow$ relates different spin-down electron configurations, equivalent to taking the system between different cluster sets. Since spin-down electrons form the boundaries of clusters, $H_\downarrow$ thus causes clusters to change in shape, merge, and divide. The states of spin-up electrons within the clusters are also changed, so matrix elements for spin-down electron hopping in this cluster language depend on the many-electron wave functions within the clusters. Taking all of these effects into account, we exactly rewrite the Hubbard Hamiltonian (for large U, projected into the single-occupancy low-energy sector) in terms of the composite cluster operators, which is then amenable to approximation and subsequent analytic exploration.

A. H_U term — Identify percolation transition

The set of real-space basis states to describe the low-energy sector of the Hubbard model for large U consists of all the ways of placing electrons into the system while avoiding double occupancy—a Gutzwiller projection [53]. Let X_σ be a set of $N_e/2$ sites hosting electrons of spin σ. Then $X_\uparrow$ and $X_\downarrow$ have no intersection, and each is a proper subset of the other's complement, i.e. $X_\uparrow \subset \overline{X_\downarrow}$ and vice versa. Any state in the basis is then specified by $X_\uparrow$ and $X_\downarrow$, and can be written as

$$|X_\uparrow, X_\downarrow\rangle = \prod_{j \in X_\uparrow} c^\dagger_{j,\uparrow} \prod_{i \in X_\downarrow} c^\dagger_{i,\downarrow} |0\rangle \,, \tag{3}$$

where $|0\rangle$ is the empty-lattice vacuum state (cf. Eq. (4) in Ref. [53]).

If we choose a state $|X_\uparrow, X_\downarrow\rangle$ from the low-energy Hilbert space at random in the thermodynamic limit then with probability 1 the positions of the electrons in the state are uncorrelated up to the single-occupancy restriction. Specifically, the probability that any site $\mathbf{x}$ is occupied by, say, a spin-down electron is given by spin-down electron density, $P(\mathbf{x} \in X_\downarrow) = n_e/2 = (1-p)/2$. Consequently, the probability that $\mathbf{x}$ *does not* contain a spin-down electron is $P(\mathbf{x} \in \overline{X_\downarrow}) = 1 - P(x \in X_\downarrow) = (1+p)/2$. The sites in $\overline{X_\downarrow}$ form clusters in the sense of a classical percolation problem as discussed in Section II, and the properties of these clusters are controlled by the "occupation" probability $P(\mathbf{x} \in \overline{X_\downarrow}) = (1+p)/2$, i.e. the probability that a site is not occupied by a spin-down electron. For small P there are only finite clusters of "not-down" sites, and for large P there is an infinite cluster of these sites. The critical point between these two regimes occurs at $P(\mathbf{x} \in \overline{X_\downarrow}) = P_c \approx 0.5927$, and we obtain a corresponding critical hole doping

$$p_c = 2P_c - 1 \approx 0.1854, \tag{4}$$

which is close to the critical hole doping $p_c \sim 0.19$ identified in experiments both as the location of the vertical feature in the experiments noted above and as the point where the pseudogap collapses in a variety of cuprate materials [54–57]. Though we have chosen spin-down electrons to bound the clusters here, breaking the symmetry between the model's treatment of the different spins, this choice is arbitrary and exchanging spin-up and spin-down everywhere yields the same results.

1. States with singly-occupied sites, for which H_U vanishes: $H_U \left|\cdots\right\rangle = 0$

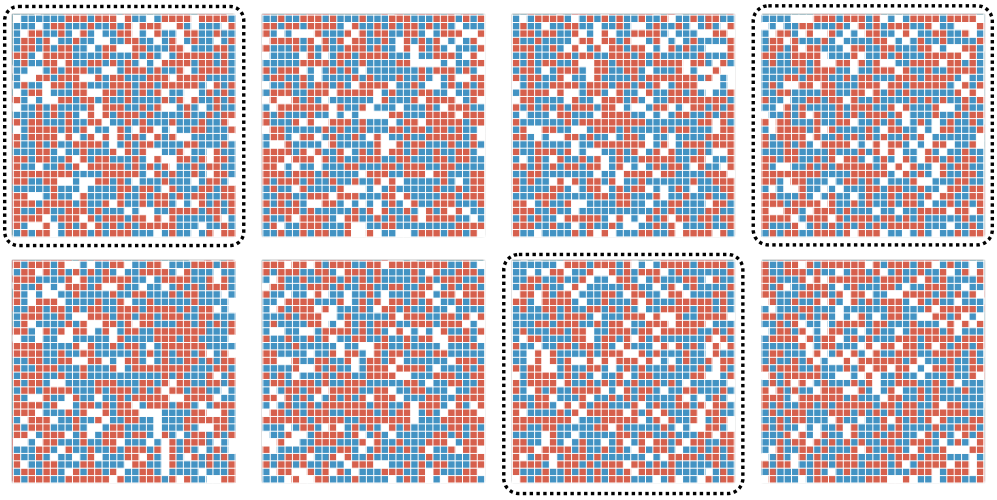

Group states with common spin-down positions (3 indicated above), defining cluster sets:

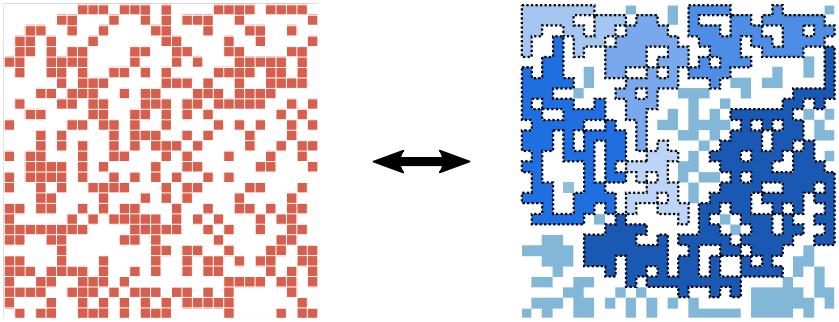

Spin-down position set $X_\downarrow$ Cluster set $\mathscr{C}$

2. For a fixed cluster set, $H_\uparrow$ acts in disjoint clusters and can be diagonalized. We change the basis for spin-up electrons from position to energy eigenstates spread over many sites, and the many-electron wave functions Ψ in each cluster are Slater determinants.

3. Spin-down hopping $H_\downarrow$relates cluster sets and gives cluster dynamics, with matrix elements determined by the wave functions of electrons within the clusters.

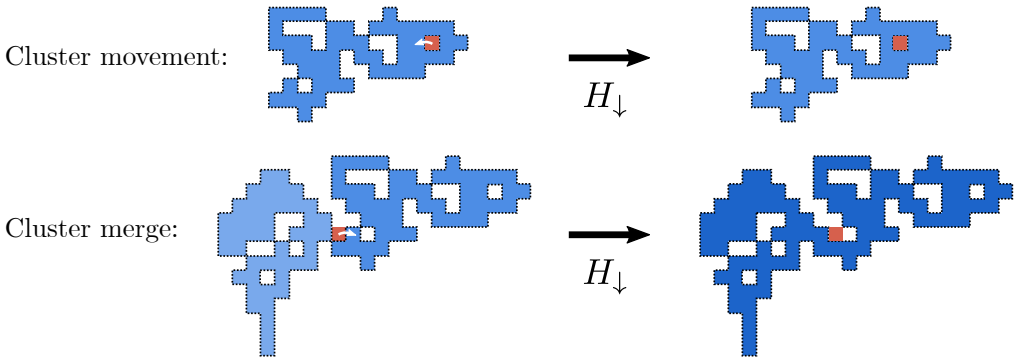

FIG. 1. A schematic representation of process of rewriting the Hubbard model implementing the percolation transition in the real-space many-electron basis states. The eight states shown at the top have only singly occupied sites, so that $H_U = 0$, with spin-up (blue sites) and spin-down (red sites) electrons placed randomly. The three states indicated with a dotted box have identical spin-down configuration $X_\downarrow$, shown below without spin-ups, which then uniquely defines a set of clusters of sites $\mathscr{C}$ where the spin-up electrons may reside. The six clusters larger than 20 sites in this example configuration are indicated. Spin-up electrons in the clusters are isolated, and $H_\uparrow$ can be diagonalized—the position basis transforms to the energy eigenbasis. Finally, we demonstrate how the hopping of a single spin-down electron via $H_\downarrow$ connects different cluster sets and produces dynamics in the clusters, such as simply shifting the center of mass of the sites in the cluster or merging clusters together.

The above argument depends on the hole doping only and is agnostic to the temperature of the system, so this p_c is independent of temperature. Note, however, that for a large but finite U virtual double occupation of sites produces a spin-spin interaction with energy scale J, that could in principle produce long-range spin correlations for $T \lesssim J$ [16]. Our focus here will be kept to higher temperatures, for which ordering from such an interaction is not favored. Additionally, any disorder in the system, be it random spatial variation of the hopping t or a random on-site potential, would also disfavor regular spatial order. Disorder is unavoidable in real systems, so the most relevant states to consider in our further analysis are precisely those without any order, manifesting the percolative behavior with T-independent transition that we have identified.

It is important to acknowledge that some experiments in the cuprates find a critical doping far from the p_c calculated above, e.g. perhaps as high as ~ 0.23 in Nd-LSCO [57–59]. The value of the percolation critical occupation probability P_c and therefore this hole doping p_c is not universal, however, so perturbations to the system will change it in general. Additionally, if we were to include a spin-spin interaction as noted above then we may need to consider a somewhat different model to make certain quantitative predictions, even at temperatures above a transition into any low-temperature ordered state. Here we use the fact that electron positions are uncorrelated to justify a classical percolation model, but a more general random cluster model [60, 61]—which has percolation, Ising, and Potts models as special cases—may be more warranted if including a spin-spin interaction in the model, and non-universal properties such as the value of p_c could change. We find that the qualitative behavior of the resistivity and optical conductivity of our system ultimately do not depend upon precise details of the percolation transition, e.g. the value of critical exponents, and rely only on the presence of a distribution of random clusters, so we proceed here with the simpler uncorrelated percolation model.

B. $H_\uparrow$ term — Cluster operators

To continue, we introduce some notation. For any state written as in Eq. (3) with a given $X_\downarrow$, we define $\mathscr{C}$ to be the set of all clusters bounded by the sites in $X_\downarrow$—it is just $\overline{X_\downarrow}$ appropriately subdivided. (See the example in Fig. 1.) Since the sets $X_\downarrow$ and $\mathscr{C}$ are in one-to-one correspondence, we will replace $X_\downarrow \to \mathscr{C}$ in our labeling of states. We consider only $p \le p_c$, so in the thermodynamic limit every $\mathscr{C}$ contains only finite clusters, which we denote as $\zeta \in \mathscr{C}$. Spin-up electrons cannot hop between clusters, so for a fixed $\mathscr{C}$ all states $|X_\uparrow, \mathscr{C}\rangle$ are block-diagonal in ζ and we have

$$|X_\uparrow, \mathscr{C}\rangle = \bigoplus_{\zeta\in\mathscr{C}} \prod_{i\in X_{\uparrow,\zeta}} c^\dagger_{i,\uparrow} |0,\zeta\rangle\,, \tag{5}$$

where $X_{\uparrow,\zeta}$ are the positions of the spin-up electrons in cluster ζ (the union of all $X_{\uparrow,\zeta}$ is $X_\uparrow$) and $|0,\zeta\rangle$ is the state with no lattice sites in the cluster occupied by spin-up electrons.

It is useful as we continue to have a way to uniquely specify any cluster ζ. One way is to list the positions of all of the sites comprising it, but this is cumbersome and will not be a useful strategy. Instead we label each cluster first with the number of sites comprising it s and the center of mass of those sites $\mathbf{r} = \sum_{i=1}^{s} \mathbf{r}_i/s$, where $\mathbf{r}_i$ are the positions of the s sites in the cluster, so that the x- and y-components of $\mathbf{r}$ are some integer multiples of a/s. Finally, let the index λ label all possible distinct shapes a cluster may have for a given s. We will denote the total number of these shapes as $N_\lambda(s)$, so that $\lambda = 1, 2, \ldots, N_\lambda(s)$ for a given s. For even relatively small s this number is large, e.g. $N_\lambda(10) = 36446$ and $N_\lambda(24) \sim 10^{13}$ [62]. The triples $\{s, \mathbf{r}, \lambda\}$ then uniquely specify each cluster—they are sufficient information to determine the positions of all s sites—and two clusters $\zeta = \{s, \mathbf{r}, \lambda\}$ and $\zeta' = \{s', \mathbf{r}', \lambda'\}$ are identical if and only if $s = s'$, $\mathbf{r} = \mathbf{r}'$, and $\lambda = \lambda'$. Sums over clusters can then be understood as summation over s, and for each s appropriate sums over $\mathbf{r}$ and λ.

In the basis of states written as Eq. (5), the spin-up hopping term of Eq. (2) becomes

$$H_\uparrow = -t \sum_{\langle ij\rangle} c^\dagger_{i,\uparrow} c_{j,\uparrow} - \mu_p \sum_i c^\dagger_{i,\uparrow} c_{i,\uparrow} = \sum_{\zeta\in\mathfrak{C}} H_\zeta \tag{6}$$

where $\mathfrak{C}$ is the set of all finite clusters appearing in *any* $\mathscr{C}$, and H_ζ is the Hamiltonian for spin-up electrons hopping inside cluster ζ. We can diagonalize each H_ζ individually,

$$H_\zeta = -t \sum_{\langle ij\rangle\in\zeta} c^\dagger_{i,\uparrow} c_{j,\uparrow} - \mu_p \sum_{i\in\zeta} c^\dagger_{i,\uparrow} c_{i,\uparrow} = \sum_{i=1}^{s} \epsilon_{\zeta,i} \psi^\dagger_{\zeta,i} \psi_{\zeta,i}, \tag{7}$$

where $\psi_{\zeta,i}$ ($\psi^\dagger_{\zeta,i}$) is the operator that destroys (creates) a spin-up electron in cluster ζ with energy $\epsilon_{\zeta,i}$, and s is the number of sites in the cluster. (For simplicity we have dropped the spin label in this basis.) These ψ's are related to the $c_\uparrow$'s as

$$c_{\mathbf{x},\uparrow} = \sum_{i=1}^{s} \phi_{\zeta,i}(\mathbf{x}) \psi_{\zeta,i}, \tag{8}$$

where $\mathbf{x}$ is the position of any of the s sites in ζ and $\phi_{\zeta,i}(\mathbf{x})$ are the wave functions for the single-particle fermionic states in the cluster. We use the convention that $\epsilon_{\zeta,i} \le \epsilon_{\zeta,j}$ if $i < j$. The energies of these single-particle states and their corresponding wave functions depend on the full geometry of the cluster, but because this is a subset of the 2d lattice we know that $|\epsilon_{\zeta,i}|$ is bounded by a scale of order t for all clusters.

With the single-particle eigenstates in each cluster we can now write definite energy multi-electron states in each cluster, and then use these to write a basis set for the whole system that diagonalizes $H_\uparrow$ for any fixed $\mathscr{C}$.

We denote the number of electrons within cluster ζ as ν_ζ ($\leq s$), and the indices of the occupied states are collected in the set $\mathcal{I}_\zeta = \{i_1, i_2, \cdots, i_{\nu_\zeta}\}$. Every possible $\mathcal{I}_\zeta$ is an element of the power set of the s total indices $\mathbb{P}_s$. The multi-fermion state in the cluster is then

$$\begin{aligned}|\mathcal{I}_\zeta, \zeta\rangle &= \psi^\dagger_{\zeta,i_{\nu_\zeta}} \cdots \psi^\dagger_{\zeta,i_1} |\varnothing, \zeta\rangle \\ &= \sum_{\{\mathbf{x}_i\}\in\zeta} \Phi_{\zeta,\mathcal{I}_\zeta}(\mathbf{x}_1, \ldots, \mathbf{x}_{\nu_\zeta})\, c^\dagger_{\mathbf{x}_{\nu_\zeta},\uparrow} \cdots c^\dagger_{\mathbf{x}_1,\uparrow} |0, \zeta\rangle\,, \end{aligned} \tag{9}$$

where $|\varnothing, \zeta\rangle$ is the state with every single-electron energy state unoccupied. (The states $|\varnothing, \zeta\rangle$ and $|0, \zeta\rangle$ both represent the vacuum, in the energy eigenbasis and position basis respectively.) The multi-fermion wave function is given by the Slater determinant

$$\Phi_{\zeta,\mathcal{I}_\zeta}(\mathbf{x}_1 \ldots \mathbf{x}_{\nu_\zeta}) = \frac{1}{\sqrt{\nu_\zeta!}} \begin{vmatrix} \phi_{\zeta,i_1}(\mathbf{x}_1) & \cdots & \phi_{\zeta,i_{\nu_\zeta}}(\mathbf{x}_1) \\ \vdots & \ddots & \vdots \\ \phi_{\zeta,i_1}(\mathbf{x}_{\nu_\zeta}) & \cdots & \phi_{\zeta,i_{\nu_\zeta}}(\mathbf{x}_{\nu_\zeta}) \end{vmatrix}, \tag{10}$$

and the total energy of this state is

$$E_{\zeta,\mathcal{I}_\zeta} = \sum_{i\in\mathcal{I}_\zeta} \epsilon_{\zeta,i}. \tag{11}$$

We can write a multi-fermion composite operator to create these states,

$$C^\dagger_{\zeta,\mathcal{I}_\zeta} = \mathcal{P}_{\zeta,\mathcal{I}_\zeta} \psi^\dagger_{\zeta,i_{\nu_\zeta}} \cdots \psi^\dagger_{\zeta,i_1}, \tag{12}$$

using the projector

$$\mathcal{P}_{\zeta,\mathcal{I}_\zeta} = \prod_{i\in\mathcal{I}_\zeta} \psi^\dagger_{\zeta,i}\psi_{\zeta,i} \prod_{j\notin\mathcal{I}_\zeta} \psi_{\zeta,j}\psi^\dagger_{\zeta,j} \prod_{\mathbf{x}\in\partial\zeta} c^\dagger_{\mathbf{x},\downarrow} c_{\mathbf{x},\downarrow}, \tag{13}$$

where $\partial\zeta$ are the sites bounding cluster ζ occupied by spin-down electrons, which ensures that C_ζ only has nontrivial action in cluster ζ and that the electrons are only put into the states indexed in $\mathcal{I}_\zeta$. The corresponding annihilation operator $C_{\zeta,\mathcal{I}_\zeta}$ can be similarly defined, and together these operators act on cluster states as

$$C^\dagger_{\zeta,\mathcal{I}_\zeta} |\varnothing, \zeta'\rangle = \delta_{\zeta,\zeta'} |\mathcal{I}_\zeta, \zeta\rangle \tag{14}$$

$$C_{\zeta,\mathcal{I}_\zeta} |\mathcal{I}'_{\zeta'}, \zeta'\rangle = \delta_{\mathcal{I}_\zeta,\mathcal{I}'_\zeta}\delta_{\zeta,\zeta'} |\varnothing, \zeta\rangle\,, \tag{15}$$

where the delta-function $\delta_{\zeta,\zeta'}$ is 1 if ζ and ζ' are the same cluster and 0 otherwise, and $\delta_{\mathcal{I}_\zeta,\mathcal{I}'_{\zeta'}}$ is 1 if the two sets are identical and 0 otherwise. The energy basis representation of Eq. (5) is then

$$|\{\mathcal{I}\}, \mathscr{C}\rangle = \bigoplus_{\zeta\in\mathscr{C}} C^\dagger_{\zeta,\mathcal{I}_\zeta} |\varnothing, \zeta\rangle\,, \tag{16}$$

where the spin-up electron position set $X_\uparrow$ is replaced with $\{\mathcal{I}\}$, the set of occupied states in each cluster. Since the total spin-up electron density is fixed to $n_e/2$, the average filling of each cluster is

$$\langle\nu_\zeta\rangle = \frac{\sum_{\zeta\in\mathscr{C}} \nu_\zeta}{\sum_{\zeta\in\mathscr{C}} s} = \frac{\frac{N_e}{2}}{N - \frac{N_e}{2}} = \frac{\frac{n_e}{2}}{1 - \frac{n_e}{2}} = \frac{1-p}{1+p} \equiv \rho_p. \tag{17}$$

Finally, with these definitions we can now rewrite the Hamiltonian in each cluster H_ζ as

$$H_\zeta = \sum_{\mathcal{I}_\zeta\in\mathbb{P}_s} E_{\zeta,\mathcal{I}_\zeta} C^\dagger_{\zeta,\mathcal{I}_\zeta} C_{\zeta,\mathcal{I}_\zeta}, \tag{18}$$

so that the spin-up hopping term of the Hubbard Hamiltonian is

$$H_\uparrow = \sum_{\zeta\in\mathfrak{C}} \sum_{\mathcal{I}_\zeta\in\mathbb{P}_s} E_{\zeta,\mathcal{I}_\zeta} C^\dagger_{\zeta,\mathcal{I}_\zeta} C_{\zeta,\mathcal{I}_\zeta}. \tag{19}$$

Notice that the parity of fermionic operators comprising $C_{\zeta,\mathcal{I}_\zeta}$ or $C^\dagger_{\zeta,\mathcal{I}_\zeta}$ is determined by the number of electrons within the cluster ν_ζ. If ν_ζ is even, then these operators are bosonic, and if ν_ζ is odd they are fermionic, and we can define

$$C_{\zeta,\mathcal{I}_\zeta} \equiv \begin{cases} b_{\zeta,\mathcal{I}_\zeta}, & \nu_\zeta \text{ even}, \\ f_{\zeta,\mathcal{I}_\zeta}, & \nu_\zeta \text{ odd}, \end{cases} \tag{20}$$

to make this difference explicit.

C. $H_\downarrow$ term — Cluster dynamics

Spin-down electrons define cluster boundaries, so when projected into the cluster basis the spin-down hopping term of Eq. (2) describes dynamics of the clusters themselves. A single spin-down hop may simply shift the center of mass (and change the shape) of a single cluster, it may cause multiple clusters to merge, or cause one cluster to divide. More concretely, the spin-down hopping term provides matrix elements between states in the Hilbert space labeled by different cluster sets $\mathscr{C}$ and $\mathscr{C}'$ that differ only in the position of a single spin-down electron. Since only a single spin-down has moved between $\mathscr{C}$ and $\mathscr{C}'$, they are the same up to only a small number of clusters; because of the geometric constraints of the square lattice at most four clusters can share a site on all of their boundaries, so all of the clusters in $\mathscr{C}$ and $\mathscr{C}'$ are identical with up to 4 exceptions.

For a spin-down electron at position $\mathbf{x}$, let N_c (≤ 4) be the number of clusters in $\mathscr{C}$ with this electron forming part of their boundary, which we will label $\zeta_1, \ldots, \zeta_{N_c}$. If this electron hops to position $\mathbf{x} + \hat{\mathbf{e}}$, where $\hat{\mathbf{e}}$ is a lattice unit vector, then it is now on the boundary of N'_c new clusters in set $\mathscr{C}'$, labeled $\zeta'_1, \ldots, \zeta'_{N'_c}$. All other clusters are unaffected, so the spin-down hopping term of the Hubbard Hamiltonian projected into the cluster basis is simply $-t$ times the inner product of the initial and

final cluster states,

$$g^{(N_c\to N_c')}_{\alpha_1'\ldots\alpha_{N_c'}';\alpha_1\ldots\alpha_{N_c}} \equiv \langle\{\mathcal{I}'\},\mathscr{C}'|\Big(\sum_{\langle ij\rangle} c^\dagger_{i,\downarrow}c_{j,\downarrow}\Big)|\{\mathcal{I}\},\mathscr{C}\rangle\,, \tag{21}$$

where we have also introduced the shorthand notation $\alpha_i = \zeta_i, \mathcal{I}_{\zeta_i}$ with associated sums

$$\sum_{\alpha_i}\cdots = \sum_{\zeta_i\in\mathfrak{C}}\sum_{\mathcal{I}_{\zeta_i}\in\mathbb{P}_{s_i}}\cdots\,. \tag{22}$$

This inner product can be expressed in terms of the multi-electron wave functions Eq. (10) for the involved clusters. Since the wave functions strongly depend on cluster shapes, these matrix elements do as well—all other indices being fixed, changing even just one of the shape indices $\lambda_1,\ldots,\lambda_{N_c}$ or $\lambda_1',\ldots,\lambda_{N_c'}'$ can significantly affect the value of the matrix element. The initial and final sets of clusters are composed of the same number of sites $s = s_1+\cdots+s_{N_c}$ with all but one in the same positions, so we can calculate the shift in the total center of mass of the sites forming the clusters—it shifts a distance a/s in the direction opposite to the spin-down hop. (See the examples in Fig. 1.) We give an explicit calculation of this matrix element in Appendix A incorporating all constraints.

The spin-down electron chemical potential term is much less complicated. No electrons are moved by this term, so in the cluster language it just takes some initial cluster configuration to itself—it contributes to the terms diagonal in cluster configuration space, like the spin-up hopping term.

D. H in terms of clusters

We can now restate the Hubbard Hamiltonian Eq. (2) for large U in terms of clusters,

$$\begin{aligned} H = &\sum_\alpha E_\alpha C^\dagger_\alpha C_\alpha - \mu_p\sum_{\{\alpha_i\}} C^\dagger_{\alpha_1}\cdots C^\dagger_{\alpha_{N_c}}C_{\alpha_{N_c}}\cdots C_{\alpha_1} \\ &- t\sum_{\{(N_c\to N_c')\}}\sum_{\{\alpha_i'\}}\sum_{\{\alpha_i\}} g^{(N_c\to N_c')}_{\alpha_1'\ldots\alpha_{N_c'}';\alpha_1\ldots\alpha_{N_c}} \\ &\qquad\times C^\dagger_{\alpha_1'}\cdots C^\dagger_{\alpha_{N_c'}'}C_{\alpha_1}\cdots C_{\alpha_{N_c}}. \end{aligned} \tag{23}$$

The first term is the entire spin-up hopping $H_\uparrow$, the second term accounts for the chemical potential part of $H_\downarrow$—the sets of N_c clusters being summed over are those which share a spin-down electron on their boundary—and the final term spanning the last two lines give the effect of spin-down electron hopping. For this to be a complete rewriting we need to identify the different allowed cluster transformations $(N_c\to N_c')$ generated by the spin-down hopping term. As noted above, we are guaranteed that there are only a finite number of these since N_c and N_c' are each restricted to be no greater than 4. In Fig. 2 we demonstrate the 8 distinct types of processes, ignoring cases where one of the involved clusters has $s = 1$ and $\nu = 0$. (We will keep only large clusters in our later approximations anyway). None involve more than 6 total clusters–4 becoming 2 or vice versa–so no term in Eq. (23) can involve more than 6 cluster operators. Even though Eq. (23) is entirely from electron kinetic energy terms, we will refer to the multi-cluster terms as interactions since they have the form of interactions between clusters.

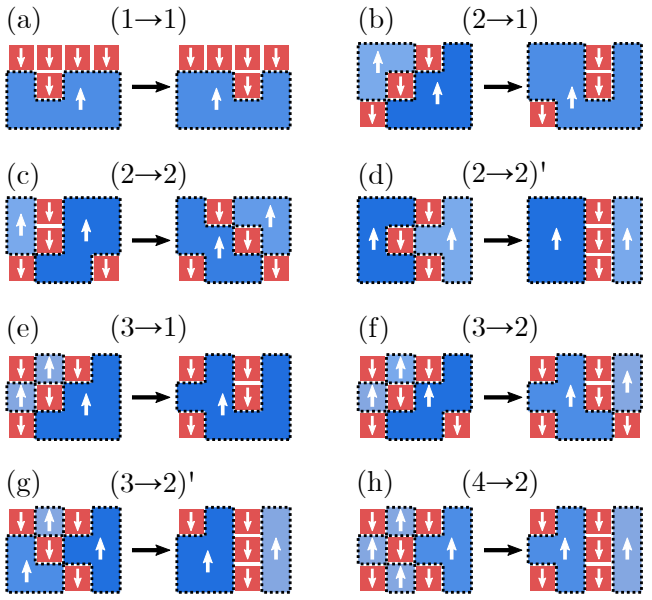

FIG. 2. Representatives of 8 distinct cluster interactions produced by the single hop of one spin-down electron (red squares with ↓), excluding processes that include empty single-site clusters. The blue regions marked with ↑ represent clusters containing the spin-up electron wave functions Φ as in Eq. (10). Processes labeled (b), (e), (f), (g), and (h) reduce the number of clusters in the system, and each have a corresponding time reversed process that increases the number of clusters. Interactions with a primed $(N_c\to N_c')$ label differ from their unprimed counterparts by containing at least one cluster that does not exchange spin-up electrons with other clusters—it's size changes by 1, but the number of occupied states within it cannot. Examples of (a) and (b) for complete clusters are also shown in Fig. 1.

IV. APPROXIMATIONS

Since Eq. (23) is equivalent to the original infinite-U Hubbard Hamiltonian it is at least as difficult to exactly calculate its properties, and to continue we must make approximations. The first approximation we make is to keep only the Gaussian $(1\to 1)$ and and 3-body $(2\to 1)$ and $(1\to 2)$ interaction terms, i.e. the $C^\dagger C$, $C^\dagger CC$, and $C^\dagger C^\dagger C$ terms. These two interactions are enough to generate all qualitatively distinct cluster dynamics—moving, changing shape, merging, and dividing. Because they require far less strict local configurations of electrons these

two interactions are far more likely to occur than any of the others, a fact supported by simple numerical simulations counting the prevalence of these local arrangements in random spin-down electron configurations for $p \sim p_c$.

In addition, finding a local configuration necessary for a many-cluster interaction does not mean that the *apparently* distinct clusters sharing the relevant boundary electron are *actually* distinct. For example, any of the apparently distinct clusters in the initial configuration shown in Fig. 2 (f) for the $(3 \to 2)$ interaction may join up outside of the depicted region, so that the hopping of the indicated electron yields an interaction of fewer clusters, and we actually have the $(2 \to 2)$, $(2 \to 1)$, or even $(1 \to 1)$ interaction. Therefore, interactions involving more clusters are even less likely than found with a naive counting of local configurations.

A. Large clusters, IR limit

We can make use of the fact that the system is near the percolation threshold to make further approximations. As noted in Section II the critical properties of the percolation transition are controlled by large clusters with sizes above some $s_0 \gg 1$, corresponding to a linear dimension $R_0 \gg a$. This provides a natural sense in which we can make an infrared approximation of this system, neglecting short length scales: we keep only $s > s_0 \gg 1$, corresponding to length scales $R > R_0 \gg a$. This restriction preserves the critical properties of the clusters, and it is reasonable to expect that it will also preserve whatever critical properties the electronic system inherits from the percolation transition.

We now start with the resulting effects of this approximation on the quantities introduced to label clusters. First, we replace sums over all discrete sizes s with integrals restricted to the range $s \in [s_0, s_\xi]$. Second, the spacing between the possible center of mass locations for large clusters is very small compared to R and even compared to the lattice scale, $\delta x = \delta y = a/s \ll a \ll R$, so we approximate sums over these positions as integrals over the 2d continuum,

$$\sum_{\mathbf{r}} \cdots \to \frac{1}{s^2} \int \mathrm{d}^2\mathbf{r} \cdots . \tag{24}$$

With this approximation all positions become indistinguishable, and quantities that depend on cluster positions lose that dependence, such as internal spectra and interaction matrix elements. Third, the number of possible cluster shapes $N_\lambda(s)$ is incredibly large for $s \geq s_0$, so anticipating an eventual infinite limit to remove terms $\sim 1/N_\lambda$, we replace it with a uniform large N_λ for all s to simplify intervening calculation.

In the large s limit, we can also make approximations to the states of spin-up electrons within the clusters. Numerical evaluation of the single-particle energies for large random clusters shows that they are well approximated by averages over shape; if $\bar{\epsilon}_{s,i}$ is the average of the energies over λ for a given s, then $|\epsilon_{\mathbf{r},s,\lambda,i} - \bar{\epsilon}_{s,i}| \ll t$. Furthermore, the average energies for different s all appear to be discrete samplings of the same continuous and gapless function, $\bar{\epsilon}_{s,i} \approx \bar{\epsilon}(i/(s+1))$. (See Appendix B for this numerical analysis.) Altogether we put

$$\epsilon_{\mathbf{r},s,\lambda,i} \approx \bar{\epsilon}(i/(s+1)) \to \bar{\epsilon}(x), \tag{25}$$

where $x \in [0,1]$ is now a continuous parameter indexing the continuum of internal states; all dependence of these energies on cluster size, shape, and position are dropped.

In this continuum approximation, the analog of the sets $\mathcal{I}$ labeling multi-electron states are now continuous occupation functions $n(x)$. When integrated over all x, the occupation function gives the fraction of occupied states, $\rho = \int \mathrm{d}x\, n(x) \approx \nu/s$. To simplify further we assume that the physically relevant case for describing the low-energy properties of the system is that of thermal occupation, so that $n(x) = n_F(\bar{\epsilon}(x) - \mu)$, where $n_F(\epsilon) = (1 + e^{\epsilon/T})^{-1}$ is the Fermi function and $\mu = \bar{\epsilon}(\rho)$ so that ρ completely characterizes the occupation of the internal states. Since the addition or removal of a single electron does not change the filling fraction in the continuum approximation, we have both a bosonic and fermionic cluster for any ρ. Finally, we will assume that all clusters have the same fraction of their states occupied, which, with the above approximations, means they are filled to the same energy, i.e. we take $\rho = \rho_p = (1-p)/(1+p)$ in all clusters, the average filling found in Eq. (17), so that $\mu = \mu_p$ in all clusters as well. For $p = p_c$ this filling is $\rho_{p_c} \approx 0.687$. The total internal energy of a cluster is then

$$E_{\mathbf{r},s,\lambda,\mathcal{I}} = \sum_{i \in \mathcal{I}} \epsilon_{\mathbf{r},s,\lambda,i} \to s \int_0^1 \mathrm{d}x\, n_F\left(\bar{\epsilon}(x) - \bar{\epsilon}(\rho_p)\right)\, \bar{\epsilon}(x) \equiv s\, E_p. \tag{26}$$

B. Interaction Matrix Elements

Averaging over cluster shapes gives an approximation of the internal spectra of clusters, but averaging over shapes is a meaningless operation for the wave functions within clusters. The wave functions of internal states are intrinsically related to cluster geometry and there are no "average wave functions" that can approximate the interaction matrix elements $g^{(N_c \to N_c')}_{\alpha' \ldots;\alpha \ldots}$. Therefore, though λ is an irrelevant index at the level of single-cluster properties, any treatment of the interactions must retain strong dependence on this degree of freedom.

First note that for large s interactions are mostly independent of s. Because of the same geometric properties that lead to the fractal relationship between cluster radius R and size s, wave functions are typically localized within some length ℓ set by the lattice scale [63–66], and moving a single site in a cluster will affect only the wave functions with weight near that site. Since the interaction matrix elements are the inner product of the wave

functions in clusters that differ by the location of a single site, only a small region of scale ℓ determines the size of any interaction amplitude. Since $R \gg \ell \sim a$ for the large clusters we consider, then the matrix elements do not strongly depend on cluster size.

With the approximations we have discussed so far the $(1 \to 1)$ interaction matrix element becomes

$$g^{(1\to1)}_{\alpha;\alpha'} \approx g_{\lambda\lambda'}\, \delta_{s,s'} \delta(\mathbf{r} - \mathbf{r}' - \hat{\mathbf{e}}/s), \tag{27}$$

where $g_{\lambda\lambda'}$ is independent of cluster position and size and encodes all shape dependence. The δ-function here gives the shift of the center of mass of the cluster—the final position $\mathbf{r}$ is shifted from the initial position $\mathbf{r}'$ by a vector of length a/s, opposite the direction of the electron hop.

A cluster can only change into a small fraction of the N_λ possible shapes by moving a single boundary electron, so for a fixed λ only a relatively small number of λ' give nonzero result. The square of the matrix elements is non-negative, so their total is some very small positive number,

$$\sum_{\lambda'} |g_{\lambda\lambda'}|^2 \equiv g^2_{2,\lambda}, \tag{28}$$

which will depend on the starting cluster shape λ. At this level we can now consider the effect of averaging over shape. The nonzero values of $g_{\lambda\lambda'}$ are just as likely to be positive as negative, so its average over shapes vanishes. We use g_2^2 for the average value of $g^2_{2,\lambda}$ over the N_λ initial cluster shapes λ, so averaging over shape indices gives

$$\langle g_{\lambda\lambda'} \rangle = 0 \tag{29}$$

$$\left\langle |g_{\lambda\lambda'}|^2 \right\rangle = \frac{1}{N_\lambda^2} \sum_{\lambda,\lambda'} |g_{\lambda\lambda}|^2 = \frac{1}{N_\lambda^2} \sum_{\lambda} g^2_{2,\lambda} = \frac{g_2^2}{N_\lambda}, \tag{30}$$

where $\langle \ldots \rangle$ denotes averaging over any unsummed shape indices. The small constant g_2^2 giving the average probability for a transition from one cluster shape to any other therefore characterizes the strength of this interaction term.

The same considerations apply directly for the $(2 \to 1)$ interaction, but with one complication—not all position dependence is removed by our approximations, and the matrix element still depends on the separation between the two initial clusters. For very large separations, much larger than the sum of the two cluster radii, two clusters are very unlikely to share a boundary so the corresponding amplitude vanishes. For very small separations they are likely to overlap, meaning they cannot both exist at once and likewise the corresponding amplitude vanishes. Only in between, in a wide window around the sum of the radii, are there separations with nonzero amplitude. Since the average cluster radius diverges near p_c we will extend this window up to the size of the system, and in the IR limit let the interaction be independent of this separation as well. We therefore have

$$g^{(2\to1)}_{\alpha';\alpha_1,\alpha_2} \approx g_{\lambda';\lambda_1\lambda_2} \delta_{s_1+s_2,s'} \delta \left(\frac{s_1}{s}\mathbf{r}_1 + \frac{s_2}{s}\mathbf{r}_2 - \mathbf{r}' - \frac{\hat{\mathbf{e}}}{s} \right) \tag{31}$$

with $g_{\lambda';\lambda_1\lambda_2}$ encoding all shape dependence of the matrix element. As in Eq. (27), the δ-function gives the shift in the total center of mass position between the initial and final clusters. Similar arguments about the properties of this quantity and the nature of the average over shapes as given for $g_{\lambda\lambda'}$ above now give

$$\begin{aligned} \langle g_{\lambda';\lambda_1\lambda_2} \rangle &= 0 \\ \left\langle |g_{\lambda';\lambda_1\lambda_2}|^2 \right\rangle &= \frac{g_3^2}{N_\lambda^2}, \end{aligned} \tag{32}$$

where g_3^2 is a positive constant characterizing the strength of this interaction. There are many fewer ways to satisfy all of the constraints of the $(2 \to 1)$ interaction than for the $(1 \to 1)$ interaction, so there are fewer nonzero values of $g_{\lambda';\lambda_1\lambda_2}$ than $g_{\lambda\lambda'}$, and $g_3^2 \ll g_2^2$.

We see that our approximations leave us with interaction constants that depend on "flavor" indices which take a large number of values and are characterized by particular statistical properties after an averaging procedure. This looks very similar to the structure posited in large-N models with random interactions such as the SYK and Yukawa-SYK models [33]. The quenched-disordered interactions in those models are self-averaging for many quantities, so considering a random fixed set of couplings gives the same result as averaging over realization of the disorder. Similarly, the specific fixed interactions that manifest in a randomly chosen state in our model are also random, and the average over cluster shapes can simply be thought of as a way to calculate quantities that are self-averaging.

C. Approximate Hamiltonian

Implementing all of the above approximations into Eq. (23), writing cluster operators explicitly as either fermionic or bosonic, and then Fourier transforming real-space cluster positions to momentum space gives

$$
\begin{aligned}
H \approx & \int_{0^+}^{s_\xi} \mathrm{d}s \int \frac{\mathrm{d}^2k}{(2\pi s)^2} \sum_{\lambda,\lambda'}^{N_\lambda} \left(s\, E_p\, \delta_{\lambda\lambda'} + \varepsilon(\mathbf{k}/s)\, g_{\lambda\lambda'}\right) C^\dagger_\lambda(\mathbf{k},s) C_{\lambda'}(\mathbf{k},s) \\
& - \mu_p \int \mathrm{d}^2k \sum_{N_c=1}^{4} m_{N_c} \prod_{i=1}^{N_c} \int_{0^+}^{s_\xi} \mathrm{d}s_i \int \frac{\mathrm{d}^2k_i}{(2\pi s_i)^2} \sum_{\lambda_i}^{N_\lambda} C^\dagger_{\lambda_i}(\mathbf{k}_i,s_i) C_{\lambda_i}(\mathbf{k}_i,s_i) \delta(\mathbf{k}-\mathbf{k}_1\cdots-\mathbf{k}_{N_c}) \\
& + \int_{0^+}^{s_\xi} \mathrm{d}s \int_{0^+}^{s} \mathrm{d}s' \int \frac{\mathrm{d}^2k}{(2\pi s)^2} \sum_{\lambda,\lambda_1,\lambda_2}^{N_\lambda} \varepsilon(\mathbf{k}/s) \Big[g^{(f;fb)}_{\lambda;\lambda_1\lambda_2} f^\dagger_\lambda(\mathbf{k},s) f_{\lambda_1}\big(\tfrac{s-s'}{s}\mathbf{k}, s-s'\big) b_{\lambda_2}\big(\tfrac{s'}{s}\mathbf{k},s'\big) \\
& \qquad + \frac{1}{2} g^{(b;ff)}_{\lambda;\lambda_1\lambda_2}\, b^\dagger_\lambda(\mathbf{k},s) f_{\lambda_1}\big(\tfrac{s-s'}{s}\mathbf{k}, s-s'\big) f_{\lambda_2}\big(\tfrac{s'}{s}\mathbf{k},s'\big) \\
& \qquad + \frac{1}{2} g^{(b;bb)}_{\lambda;\lambda_1\lambda_2}\, b^\dagger_\lambda(\mathbf{k},s) b_{\lambda_1}\big(\tfrac{s-s'}{s}\mathbf{k}, s-s'\big) b_{\lambda_2}\big(\tfrac{s'}{s}\mathbf{k},s'\big) \Big] + \text{h.c.},
\end{aligned}
\tag{33}
$$

where $\varepsilon(\mathbf{k}/s) = -2t\left[\cos(k_x a/s) + \cos(k_y a/s)\right]$ results from the δ-functions in Eqs. (27) and (31) and the Fourier transform, m_{N_c} is the average number of boundary spin-down electrons shared by N_c clusters, and the factor of s^{-2} coming with the momentum integrals is from the continuum limit of the original position sums. We have also extended the size variables down to 0, and only use the explicit cutoff $s_0 > 0$ when necessary to avoid unphysical divergences stemming from this approximation. The interaction constants are labeled to indicate the parity of operators they appear with. Exchange statistics in the 3-cluster interactions requires that

$$
g^{(b;ff)}_{\lambda;\lambda_1\lambda_2} = -g^{(b;ff)}_{\lambda;\lambda_2\lambda_1} \quad \text{and} \quad g^{(b;bb)}_{\lambda;\lambda_1\lambda_2} = g^{(b;bb)}_{\lambda;\lambda_2\lambda_1}. \tag{34}
$$

In Eq. (21) these conditions naturally arise from the (anti)symmetry of the underlying wave functions. The factors of 1/2 in the last two terms of the Hamiltonian account for double counting from these symmetries.

The averages of the three-cluster coefficients are

$$
\begin{aligned}
\left\langle g^{(f;fb)}_{\lambda;\lambda_1\lambda_2} \right\rangle &= \left\langle g^{(b;ff)}_{\lambda;\lambda_1\lambda_2} \right\rangle = \left\langle g^{(b;bb)}_{\lambda;\lambda_1\lambda_2} \right\rangle = 0 \\
\left\langle g^{(f;fb)\dagger}_{\lambda;\lambda_1\lambda_2}\, g^{(f;fb)}_{\lambda';\lambda_1'\lambda_2'} \right\rangle &= \frac{g_3^2}{N_\lambda^2} \delta_{\lambda\lambda'}\delta_{\lambda_1\lambda_1'}\delta_{\lambda_2\lambda_2'} \\
\left\langle g^{(b;\eta\eta)\dagger}_{\lambda;\lambda_1\lambda_2}\, g^{(b;\eta\eta)}_{\lambda';\lambda_1'\lambda_2'} \right\rangle &= \frac{g_3^2}{N_\lambda^2} \delta_{\lambda\lambda'} \left(\delta_{\lambda_1\lambda_1'}\delta_{\lambda_2\lambda_2'} + a\delta_{\lambda_1\lambda_2'}\delta_{\lambda_2\lambda_1'}\right),
\end{aligned}
\tag{35}
$$

where $\eta = f$ or b, and are all characterized by the same g_3^2. The only difference between the three corresponding terms in the Hamiltonian is the presence or absence of an extra electron inside one of the initial or final clusters, which is insignificant for large clusters.

With all of our approximations the term of Eq. (33) giving the internal cluster energy from spin-up electrons can be expressed in terms of the density of critical clusters,

$$
\begin{aligned}
E_\uparrow &= \int_{s_0}^{s_\xi} \mathrm{d}s \int \frac{\mathrm{d}^2k}{(2\pi s)^2} \sum_{\lambda=1}^{N_\lambda} s\, E_p \left\langle C^\dagger_\lambda(\mathbf{k},s) C_\lambda(\mathbf{k},s) \right\rangle \\
&= E_p \int_{s_0}^{s_\xi} \mathrm{d}s\, s\, n_s \propto p_c E_p.
\end{aligned}
\tag{36}
$$

For any given p this and the term proportional to μ_p are simply constant shifts of the total energy and we drop both from further consideration.

D. Peierls Substitution

To calculate transport properties we must determine how the to couple the model to an external electromagnetic field. Electrons in the original lattice model can be coupled to an electromagnetic field with a Peierls substitution,

$$
t \to t\, \exp\left[ie \int_{\mathbf{r}}^{\mathbf{r}+a\hat{\mathbf{e}}} \mathrm{d}\mathbf{l} \cdot \mathbf{A}(\mathbf{l}) \right], \tag{37}
$$

where $\mathbf{r}$ is the initial position of the electron, the unit vector $\hat{\mathbf{e}} \in \{\pm\hat{\mathbf{e}}_x, \pm\hat{\mathbf{e}}_y\}$ gives the direction along which it hops, e is the electron charge, and $\mathbf{A}$ is the vector potential. We will take a spatially uniform but time dependent $\mathbf{A}$ producing a uniform electric field. We then carry through the same approximations as above with this new phase factor. Just as we discard the internal energy term, we also neglect the coupling of $\mathbf{A}$ to the electrons within clusters. The terms we keep reflect the coupling of the electromagnetic field to clusters' dynamics rather than just their internal states and allow us to calculate the clusters' electromagnetic properties.

The result is that the electromagnetic field enters via minimal coupling $\varepsilon(\mathbf{k}) \to \varepsilon(\mathbf{k} - e\mathbf{A})$, and expansion in powers of e lets us treat its effect perturbatively. To $O(e^2)$ the full Hamiltonian including the coupling to $\mathbf{A}$ can thus be obtained from Eq. (33) by putting

$$
\varepsilon(\mathbf{k}) \to \varepsilon(\mathbf{k}) - e\, A_i \frac{\partial \varepsilon(\mathbf{k})}{\partial k_i} + \frac{e^2}{2} A_i A_j \frac{\partial^2 \varepsilon(\mathbf{k})}{\partial k_i \partial k_j}, \tag{38}
$$

where repeated indices are summed. Because the function $\varepsilon(\mathbf{k})$ appears with each interaction we acquire two new terms for each cluster interaction, a paramagnetic term at $O(e)$ and a diamagnetic term at $O(e^2)$.

V. MODEL ACTION

Using the approximated form of the Hamiltonian, we now write a model Matsubara action. To start, if we redefine the cluster operators in Eq. (33) as $f_\lambda(\mathbf{k}, s) \to f_\lambda(\mathbf{k}/s, s)$, and similarly for b, then all operators have the same $\mathbf{k}/s$ momentum argument. In fact the momentum appears only in this way, so we can rescale momentum and remove this common factor of s. We then promote the operators to fields $\psi^\eta_\lambda(\tau, \mathbf{k}, s)$ as functions of imaginary time τ, labeling bosonic and fermionic cluster fields by their respective statistical signs $\eta = \pm$. The resulting action is

$$\begin{aligned} S \approx & \int_{0^+}^{s_\xi} \mathrm{d}s \int_0^{1/T} \mathrm{d}\tau \int \frac{\mathrm{d}^2 k}{(2\pi)^2} \sum_{\lambda,\lambda'=1}^{N_\lambda} \sum_{\eta=\pm} \bar{\psi}^\eta_\lambda(\tau, \mathbf{k}, s) \left[(\partial_\tau - \mu_\eta(s)) \frac{\delta_{\lambda\lambda'}}{N_\lambda} + g_{\lambda\lambda'}\, \varepsilon(\mathbf{k}) \right] \psi^\eta_{\lambda'}(\tau, \mathbf{k}, s) \\ & + \int_{0^+}^{s_\xi} \mathrm{d}s \int_{0^+}^{s} \mathrm{d}s' \int_0^{1/T} \mathrm{d}\tau \int \frac{\mathrm{d}^2 k}{(2\pi)^2} \sum_{\lambda,\lambda_1,\lambda_2}^{N_\lambda} \varepsilon(\mathbf{k}) \Big[g^{(f;fb)}_{\lambda;\lambda_1,\lambda_2}\, \bar{\psi}^-_\lambda(\tau, \mathbf{k}, s) \psi^-_{\lambda_1}(\tau, \mathbf{k}, s - s') \psi^+_{\lambda_2}(\tau, \mathbf{k}, s') \\ & \qquad + \frac{1}{2} g^{(b;ff)}_{\lambda;\lambda_1,\lambda_2}\, \bar{\psi}^+_\lambda(\tau, \mathbf{k}, s) \psi^-_{\lambda_1}(\tau, \mathbf{k}, s - s') \psi^-_{\lambda_2}(\tau, \mathbf{k}, s') \\ & \qquad + \frac{1}{2} g^{(b;bb)}_{\lambda;\lambda_1,\lambda_2}\, \bar{\psi}^+_\lambda(\tau, \mathbf{k}, s) \psi^+_{\lambda_1}(\tau, \mathbf{k}, s - s') \psi^+_{\lambda_2}(\tau, \mathbf{k}, s') \Big] + \text{h.c.}, \end{aligned} \tag{39}$$

where $\mu_\pm(s)$ are chemical potentials (unrelated to μ_p in Eq. (2)) introduced to fix the boson and fermion densities to the cluster number scaling form, $n(s) = n_0 s^{-\tau_P}$ for the range of s we consider where n_0 is a proportionality constant. We can express the terms of this action diagrammatically as shown in Fig. 3. The Gaussian propagators are represented as single solid or dashed lines for fermions and bosons respectively. With the analogy between our interactions and the random disordered interactions of large-N models, each interaction is associated with a dotted "disorder" line ending in $\times$, and sensible diagrams with nonzero averages are made by connecting two $\times$'s from the same type of vertex, representing an average over the square of one of the g's.

A. Dyson equation

To calculate properties of this model we first need the Green's functions for fermionic and bosonic cluster fields. To proceed we transform to Matsubara frequencies $\omega_n = [2n + (1 \mp 1)/2]\pi T$, and identify the non-interacting Green's functions

$$G_{0,\pm}(i\omega_n, s) = \frac{1}{i\omega_n + \mu_\pm(s)}. \tag{40}$$

These are independent of momentum and flavor index, and depend on s only through the chemical potentials.

As for other large-N models, interaction contributions are dominated by terms that do not have crossed disorder lines in their diagrammatic representation, for example melon diagrams in the SYK model. The diagrammatic expansion of the Green's functions for our model are shown in Fig. 4 and give the Dyson equation

$$G_\pm(i\omega_n, \mathbf{k}, s)^{-1} = i\omega_n + \mu_\pm(s) - \Sigma_\pm(i\omega_n, \mathbf{k}, s), \tag{41}$$

where the self-energies $\Sigma_\pm$ are most easily written in terms of imaginary time as

$$\begin{aligned} \Sigma_-(\tau, \mathbf{k}, s) = & \, g_2^2\, \varepsilon(\mathbf{k})^2 G_-(\tau, \mathbf{k}, s) \\ & - g_3^2\, \varepsilon(\mathbf{k})^2 \left[\int_{0^+}^{s} \mathrm{d}s' G_+(\tau, \mathbf{k}, s') G_-(\tau, \mathbf{k}, s - s') + \int_{0^+}^{s_\xi - s} \mathrm{d}s' \sum_{\eta=\pm} \eta\, G_\eta(-\tau, \mathbf{k}, s') G_{-\eta}(\tau, \mathbf{k}, s + s') \right], \end{aligned} \tag{42}$$

$$\begin{aligned} \Sigma_+(\tau, \mathbf{k}, s) = & \, g_2^2\, \varepsilon(\mathbf{k})^2 G_+(\tau, \mathbf{k}, s) \\ & - g_3^2\, \varepsilon(\mathbf{k})^2 \left[\frac{1}{2} \int_{0^+}^{s} \mathrm{d}s' \sum_{\eta=\pm} G_\eta(\tau, \mathbf{k}, s') G_\eta(\tau, \mathbf{k}, s - s') + \int_{0^+}^{s_\xi - s} \mathrm{d}s' \sum_{\eta=\pm} \eta\, G_\eta(-\tau, \mathbf{k}, s') G_\eta(\tau, \mathbf{k}, s + s') \right]. \end{aligned} \tag{43}$$

Explicit dependence on s is acquired in the g_3^2 terms from the integrals over s'.

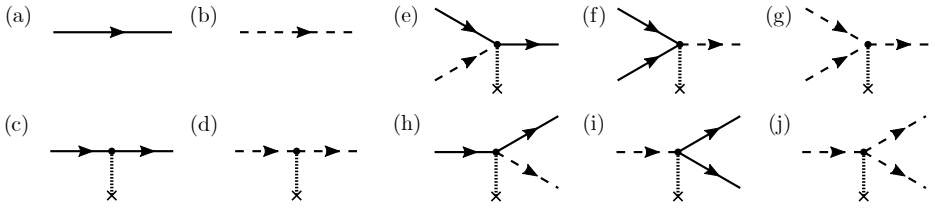

FIG. 3. The diagrammatic representation of the terms of our model action, Eq. (39). The solid line (a) is the bare fermionic propagator and dashed line (b) is bare bosonic propagator. The random Gaussian terms are given in (c) for fermions and (d) for bosons. The 3-body interactions and their Hermitian conjugates are given in (e) through (j). Each • vertex contributes a factor of $\varepsilon(\mathbf{k})$ and the corresponding g. Dotted lines in the interaction diagrams terminating in $\times$ represent "disorder lines" for each vertex, and connecting two of these gives the average of a square of the corresponding g.

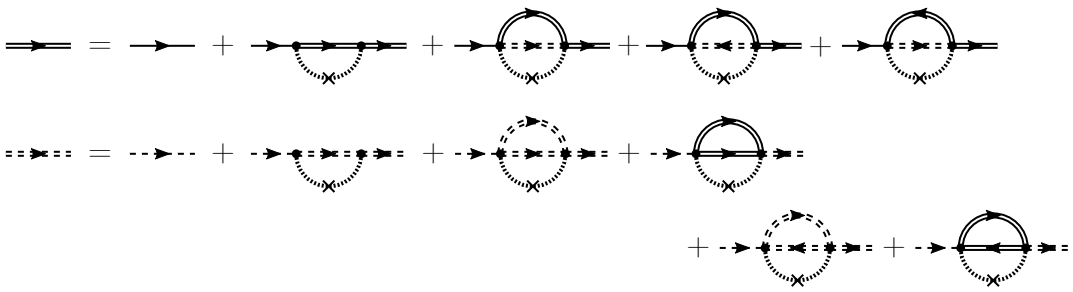

FIG. 4. The diagrammatic representation of the full Green's functions, represented here as double solid (fermionic) or double dashed (bosonic) lines. Other elements are the same as in Fig. 3. From these diagrams we can write the Dyson equation Eq. (41) with self-energies as in Eqs. (42) and (43).

We now consider two qualitatively distinct parameter regimes for this set of equations: one where the terms with coefficient g_2^2 dominate the self-energy (Gaussian regime), and one where the terms with coefficient g_3^2 dominate (cubic regime). We label quantities in the first case with a subscript 2 and in the latter case with a subscript 3, so that

$$G_{2,\pm}(i\omega_n,\mathbf{k},s)^{-1} = i\omega_n + \mu_\pm(s) - \Sigma_{2,\pm}(i\omega_n,\mathbf{k},s) \quad (44)$$

$$\Sigma_{2,\pm}(i\omega_n,\mathbf{k},s) = g_2^2\,\varepsilon(\mathbf{k})^2 G_{2,\pm}(i\omega_n,\mathbf{k},s), \quad (45)$$

and similarly for $G_{3,\pm}$ with $\Sigma_{3,\pm}$ given by the g_3^2 terms in Eqs. (42) and (43).

B. Gaussian solution — G_2

At the Gaussian level the bosonic and fermionic sectors of the theory have the same form and do not couple so $G_{2,+}$ and $G_{2,-}$ must also have the same form. Because $\Sigma_{2,\pm}$ is proportional to $G_{2,\pm}$, we have a quadratic equation for the Green's function and the solution is easily obtained. Continued from Matsubara frequency to generic complex frequency z we have

$$G_{2,\pm}(z-\mu_\pm(s),\mathbf{k},s) = \frac{2}{z + \operatorname{sgn}\left[\operatorname{Re}(z)\right]\sqrt{z^2 - 4g_2^2\,\varepsilon(\mathbf{k})^2}}, \quad (46)$$

where the sign before the square root ensures that $G_2(z) \sim 1/|z|$ for large $|z|$.

Restricting to $z = \omega + i0$ gives the retarded Green's functions,

$$G^R_{2,\pm}(\omega-\mu_\pm(s),\mathbf{k},s) = \frac{\Theta(\omega^2 - 4g_2^2\,\varepsilon(\mathbf{k})^2)}{\frac{\omega}{2} + \operatorname{sgn}(\omega)\sqrt{\left(\frac{\omega}{2}\right)^2 - g_2^2\,\varepsilon(\mathbf{k})^2}} + \left(\frac{\omega}{2} - i\sqrt{g_2^2\,\varepsilon(\mathbf{k})^2 - \left(\frac{\omega}{2}\right)^2}\right)\frac{\Theta(4g_2^2\,\varepsilon(\mathbf{k})^2 - \omega^2)}{g_2^2\,\varepsilon(\mathbf{k})^2} \quad (47)$$

shown in Fig. 5, and the spectral densities are

$$\rho_{2,\pm}(\omega,\mathbf{k}) = -\frac{1}{\pi}\operatorname{Im} G^R_{2,\pm}(\omega-\mu_\pm(s),\mathbf{k},s) = \frac{\sqrt{g_2^2\,\varepsilon(\mathbf{k})^2 - \left(\frac{\omega}{2}\right)^2}}{\pi\, g_2^2\,\varepsilon(\mathbf{k})^2}\Theta\left(4g_2^2\,\varepsilon(\mathbf{k})^2 - \omega^2\right). \quad (48)$$

Notice that the range of support for the spectral density depends on $\varepsilon(\mathbf{k}) = -2t\left[\cos(k_x a) + \cos(k_y a)\right]$, and that this range is widest for $\mathbf{k}_0 = (0,0)$ and $\mathbf{k}_\pi = (\pi/a, \pi/a)$, both giving $|\varepsilon(\mathbf{k})| = 4t$.

Using these spectral densities we can write the bosonic and fermionic cluster densities,

$$n_\pm(s) = \int \frac{\mathrm{d}^2k}{(2\pi)^2}\int \mathrm{d}\omega\, \rho_{2,\pm}(\omega,\mathbf{k})\, n_{B/F}(\omega-\mu_a(s)), \quad (49)$$

where $n_{B/F}(\omega) = 1/(e^{\omega/T} \mp 1)$ are the Bose and Fermi functions. We can now fix the chemical potentials by

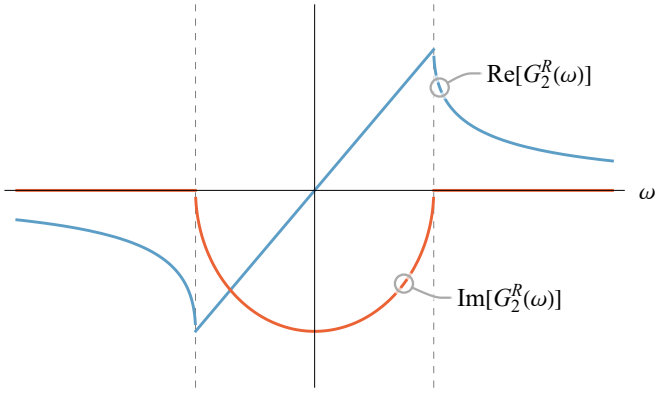

FIG. 5. A plot of the real and imaginary parts of the retarded Gaussian sector Green's functions $G^R_{2,\pm}$, Eq. (47). The vertical dashed lines indicate where $|\omega + \mu_\pm| = 2g_2|\varepsilon(\mathbf{k})|$.

ensuring these densities are consistent with the behavior demanded by percolation. Since $n(s)$ is small for the range of s we are considering, both $n_+(s)$ and $n_-(s)$ must also be small. Therefore, for $T \ll 4t$ only the states near the momenta $\mathbf{k}_{0,\pi}$ are relevant—if we integrate $\rho_{2,\pm}(\omega, \mathbf{k})$ over all momenta, the lowest ω giving nonzero values only have contributions near $\mathbf{k}_{0,\pi}$. We expand $\varepsilon(\mathbf{k})$ around these points, giving a quadratic dispersion in each case,

$$\varepsilon(\mathbf{k}_0 + \mathbf{p}) = -\varepsilon(\mathbf{k}_\pi + \mathbf{p}) \approx \frac{p^2}{2m} - 4t \equiv \varepsilon(p), \tag{50}$$

where the effective mass is defined as $m \equiv 1/(2ta^2)$ and this parabolic approximation is cut off at an energy scale $\Lambda \sim t$. Assuming that $T \gg g_2 t$, consistent with $T \ll 4t$ since $g_2 \ll 1$, we find

$$\mu_+(s) \approx -2T \operatorname{arcoth}\left(1 + \frac{n_+(s)}{n_\Lambda}\right) \tag{51}$$

$$\mu_-(s) \approx -2T \operatorname{artanh}\left(1 - \frac{n_-(s)}{n_\Lambda}\right), \tag{52}$$

where n_Λ is the density associated with the cutoff scale, much larger than $n_\pm(s)$.

C. Cubic solution — G_3

Our analysis in the cubic regime is similar to the treatment of the SYK model for complex fermions, e.g. as in Refs. [34, 67]. (For details of this full calculation see Appendix C). We first assume that the self-energies $\Sigma_{3,\pm}$ dominate over the linear-in-frequency term of the Dyson equation, which will partially restrict the regime in which the resulting solution applies. Then the form of the self-energies motivates us to consider a scaling ansatz for $G_{3,\pm}$ in the zero temperature limit, and for complex frequency z (with $\mathrm{Im}(z) > 0$) we put

$$G_{3,\pm}(z, \mathbf{k}, s) = s^{\gamma_\pm} \frac{e^{-i(\pi\Delta_\pm + \theta_\pm(s))}}{\Omega_\pm(\mathbf{k})^{2\Delta_\pm} z^{1-2\Delta_\pm}}, \tag{53}$$

where $\gamma_\pm$ and $\Delta_\pm$ are real exponents characterizing the scaling with s and frequency respectively, $\Omega_\pm(\mathbf{k})$ are energies introduced to fix dimensions and account for momentum dependence, and $\theta_\pm(s)$ parameterize the spectral asymmetry and consequently the finite density for each s—they are in principle related to $\mu_\pm(s)$ which fix the density in the non-scaling regime.

Positivity of the spectral densities gives the constraints $\pi\Delta_+ \le \theta_+(s) \le \pi(1 - \Delta_+)$ and $-\pi\Delta_- \le \theta_-(s) \le \pi\Delta_-$. Furthermore, since the density $n(s)$ vanishes for $s > s_\xi$, we take the functions $\theta_\pm(s)$ to depend on s_ξ itself and on s only through s/s_ξ, and we substitute $\theta_\pm(s) \to \theta_\pm(s/s_\xi)$. Transforming to imaginary time τ the ansatz becomes

$$G_{3,\pm}(\tau, \mathbf{k}, s) = -\operatorname{sgn}(\tau) \frac{s^{\gamma_\pm}\Gamma(2\Delta_\pm)}{\pi\Omega_\pm(\mathbf{k})^{2\Delta_\pm}|\tau|^{2\Delta_\pm}} \times \sin\left[\pi\Delta_\pm + \operatorname{sgn}(\tau)\theta_\pm(s/s_\xi)\right], \tag{54}$$

where $\Gamma(x)$ is the gamma function.

We assume that the self-energies evaluated at zero frequency cancel against the chemical potentials in Eq. (41), $\Sigma_\pm(0, \mathbf{k}, s) = \mu_\pm(s)$. Then substituting the ansatz we find that consistency of the $s \to 0^+$ and $s = s_\xi$ limits of the Dyson equation constrain many of our parameters: we obtain exponents $\Delta_+ = \Delta_- = 1/3$ and $\gamma_+ = \gamma_- = -1/3$, and find $\Omega_+(\mathbf{k}) \propto \Omega_-(\mathbf{k}) \propto |\varepsilon(\mathbf{k})|$. The constants $c_\pm$ that can be introduced to exactly relate $\Omega_\pm(\mathbf{k})$ to $\varepsilon(\mathbf{k})$ are $O(1)$ numbers given by integrals over functions of $\theta_\pm(s/s_\xi)$.

Altogether we have

$$G_{3,\pm}(z, \mathbf{k}, s) = \frac{e^{-i(\pi/3 + \theta_\pm(s/s_\xi))}}{c_\pm^{2/3}\, g_3^{2/3}\, s^{1/3}\, \varepsilon(\mathbf{k})^{2/3}\, z^{1/3}}, \tag{55}$$

the same form for both bosonic and fermionic fields. Taking $z \to \omega + i0$ we acquire the retarded Green's function,

$$G^R_{3,\pm}(\omega, \mathbf{k}, s) = \operatorname{sgn}(\omega) \frac{e^{-i(\operatorname{sgn}(\omega)\pi/3 + \theta_\pm(s/s_\xi))}}{c_\pm^{2/3}\, g_3^{2/3}\, s^{1/3}\, \varepsilon(\mathbf{k})^{2/3} |\omega|^{1/3}}. \tag{56}$$

To obtain this solution we have assumed first that we are in a parameter regime where the Gaussian terms in the self-energies are much smaller than the cubic terms, and second that $|\Sigma_{3,\pm}| = \left|G^{-1}_{3,\pm}\right| \gg |\omega|$ for nonzero frequency. These constrain the frequency regime for which $G_{3,\pm}$ applies to be

$$\frac{g_2^3}{s\,\tilde{g}_3^2}|\varepsilon(\mathbf{k})| \ll |\omega| \ll \sqrt{s}\,\tilde{g}_3\,|\varepsilon(\mathbf{k})|. \tag{57}$$

Since we are interested large s we therefore find that this power-law Green's function may apply over a finite range of frequencies, not just in the limit of zero frequency as is the typical case for the SYK model—indeed, this solution *never* applies for zero frequency, and in that limit we must use G_2 as found in Section V B; s_ξ is always cut off at some large value in a finite system, so the regime of applicability for G_3 never extends down to include $\omega = 0$.

VI. TRANSPORT PROPERTIES

The coupling of the cluster fields to a spatially-uniform electromagnetic field in the action Eq. (39) is obtained via minimal coupling as in Section IV D for the Hamiltonian description, but now we take the vector potential to be a function of imaginary time $\mathbf{A}(\tau)$. The electromagnetic linear response function $\hat{\Pi}(i\omega_n)$ can be calculated in the usual way as the second derivative with respect to $\mathbf{A}$ of the partition function constructed from the action S including the coupling to $\mathbf{A}$. The result is greatly simplified because of the large-N nature of the theory and the averaging procedure. First, there are no contributions at first order in an interaction constant since $\langle g_{\ldots}\rangle = 0$. Therefore, the two types of diagrams contributing to $\hat{\Pi}$ are bubble diagrams with two paramagnetic vertices or with one diamagnetic vertex and one normal interaction vertex. Second, vertex corrections necessitate crossed disorder lines, which contribute at $O(1/N_\lambda)$, and so vanish in the large-N_λ limit. Finally, because $g_2^2 \gg g_3^2$ the primary contribution comes from the coupling of the Gaussian terms in the action to $\mathbf{A}$, so $\hat{\Pi}$ has an overall factor of g_2^2. Taking these points into account the effect of diagrams higher order in g_2 and g_3 is simply to dress the bare propagators as in Fig. 4, so $\hat{\Pi}$ can be represented diagrammatically as in Fig. 6, and we have

$$\Pi_{ij}(i\omega_n) \approx e^2 g_2^2\, T \int \mathrm{d}s \int \frac{\mathrm{d}^2k}{(2\pi)^2} \sum_{\eta=\pm} \sum_{\{\omega_n'\}} \times \left(\frac{\partial\varepsilon(\mathbf{k})}{\partial k_i}\frac{\partial\varepsilon(\mathbf{k})}{\partial k_j} G_\eta(i\omega_n', \mathbf{k}, s) G_\eta(i\omega_n' - i\omega_n, \mathbf{k}, s) + \varepsilon(\mathbf{k}) \frac{\partial^2\varepsilon(\mathbf{k})}{\partial k_i \partial k_j} G_\eta(i\omega_n', \mathbf{k}, s)^2 \right). \quad (58)$$

The optical conductivity is defined using the retarded response, obtained from this via analytic continuation $i\omega_n \to \omega + i0$. Since the model is isotropic and we are interested in its longitudinal transport properties, we further define the longitudinal response function as the average of the diagonal elements of this matrix, $\Pi = (\Pi_{xx} + \Pi_{yy})/2$.

Even though the Gaussian couplings to $\mathbf{A}$ dominate Π, the Green's functions appearing in Eq. (58) may have either Gaussian G_2 or cubic G_3 form; whether the Gaussian or cubic self-energies dominate the Dyson equation depends on the frequency regime being considered, not the relative sizes of g_2 and g_3. When evaluating the Matsubara sum in the standard way via contour integration the different analytic structures of G_2 and G_3 become vitally important and each case must be considered separately. As previously noted, when continued to real frequencies G_3 is applicable in a range of finite frequencies excluding $\omega = 0$, so that G_2 is relevant for the dc limit.

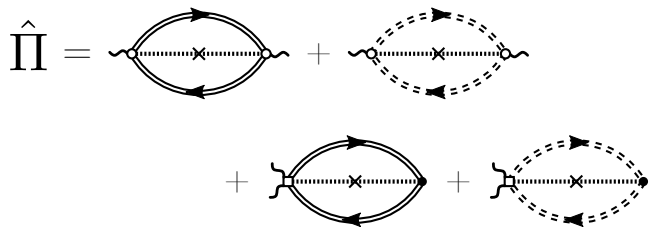

FIG. 6. The diagrams giving the response of the effective theory to an external electromagnetic field, dropping all contributions $O(1/N_\lambda)$ or smaller. The open circles with a single $\sim$ represent paramagnetic coupling to $\mathbf{A}$ and the squares with two $\sim$'s represent diamagnetic coupling to $\mathbf{A}^2$. The propagators (double solid or dashed lines) are dressed by interactions as in Fig. 4. All other diagrams vanish with the disorder average or have crossed impurity lines and so vanish in the $N_\lambda \to \infty$ limit.

A. Linear-in-T Resistivity

The dc resistivity ρ is the reciprocal of the dc conductivity σ, which itself is the real part of the $\omega \to 0$ limit of the optical conductivity. In terms of Π,

$$\sigma = \mathrm{Re}\left[\lim_{\omega\to 0}\sigma(\omega)\right] = \mathrm{Re}\left[\lim_{\omega\to 0}\frac{\Pi(\omega + i0)}{i\omega}\right]. \quad (59)$$

After rewriting the Matsubara sums in the expression for Π in terms of integrals over real frequencies of Fermi and Bose distribution functions and functions of retarded and advanced Green's functions we have

$$\sigma = \mathrm{Re}\left\{ -\frac{e^2 g_2^2}{4\pi} \int \mathrm{d}s \int \frac{\mathrm{d}^2k}{(2\pi)^2} |\boldsymbol{\nabla}_k \varepsilon(\mathbf{k})|^2 \sum_{\eta=\pm} \int \mathrm{d}\omega' n_a(\omega') \lim_{\omega\to 0}\frac{1}{\omega}\left[G_\eta^R(\omega') - G_\eta^A(\omega')\right]\left[G_\eta^R(\omega'+\omega) + G_\eta^A(\omega'-\omega)\right] - \lim_{\omega\to 0}\frac{1}{\omega}\frac{e^2 g_2^2}{4\pi}\int \mathrm{d}s \int \frac{\mathrm{d}^2k}{(2\pi)^2}\varepsilon(\mathbf{k})\boldsymbol{\nabla}_k^2\varepsilon(\mathbf{k}) \sum_{\eta=\pm}\int \mathrm{d}\omega' n_a(\omega')\left[G_\eta^R(\omega')^2 - G_\eta^A(\omega')^2\right] \right\}, \quad (60)$$

where we have suppressed the Green's functions' common dependence on $\mathbf{k}$ and s. In this regime the relevant Green's functions are the zero-frequency limit of $G_{2,\pm}$ as in Eq. (47) with the chemical potentials $\mu_\pm(s,T)$ as in

Eqs. (51) and (52). Because of the branch cut in these Green's functions for small frequencies, the integral over the integrated frequency ω' is restricted to the range $-2g_2|\varepsilon(\mathbf{k})| - \mu_\pm(s) \leq \omega' \leq 2g_2|\varepsilon(\mathbf{k})| - \mu_\pm(s)$; contributions from outside this range exactly cancel. Because of the $\omega \to 0$ limit we expand the Green's functions in the first line in powers of ω. The 0th order terms of this expansion, which simply evaluates the Green's functions at $\omega = 0$, are overall proportional to $1/\omega$ and combine with the second line. Using the form of $G^R_{2,\pm}$ and $G^A_{2,\pm} = (G^R_{2,\pm})^*$, these terms are found to contribute a purely imaginary Drude term $\propto 1/(i\omega)$ as expected from a model with translational symmetry. We will not analyze here how or if this term is removed by the inclusion of disorder in the system, as is typically the case, and will continue keeping just the real part of the conductivity. Of the remaining terms in the expansion of the Green's functions only the terms first order in ω survive in the $\omega \to 0$ limit, and will be our focus from here on.

The Green's functions in the remaining real term enter in the form

$$\left[G^R_{\pm,2}(\omega') - G^A_{\pm,2}(\omega')\right]\left[\frac{\mathrm{d}G^R_{\pm,2}(\omega')}{\mathrm{d}\omega'} - \frac{\mathrm{d}G^A_{\pm,2}(\omega')}{\mathrm{d}\omega'}\right] = \frac{1}{2}\frac{\mathrm{d}}{\mathrm{d}\omega'}\left[G^R_{\pm,2}(\omega') - G^A_{\pm,2}(\omega')\right]^2 = \frac{\omega' + \mu_\pm(s)}{g_2^4 \varepsilon(\mathbf{k})^4}, \quad (61)$$

where the last equality uses the form of the Green's function in this frequency range, Eq. (47). With a shift of the integrated frequency by the chemical potential the dc conductivity becomes

$$\sigma = -\frac{e^2}{4\pi g_2^2}\int \mathrm{d}s \int \frac{\mathrm{d}^2k}{(2\pi)^2}\frac{|\boldsymbol{\nabla}_k \varepsilon(\mathbf{k})|^2}{\varepsilon(\mathbf{k})^4} \times \sum_{\eta=\pm}\int_{-2g_2|\varepsilon(\mathbf{k})|}^{2g_2|\varepsilon(\mathbf{k})|} \mathrm{d}\omega'\, \omega'\, n_\eta\left[\omega' - \mu_\eta(s)\right], \quad (62)$$

and we can evaluate the frequency integral using the chemical potentials given in Eqs. (51) and (52). Since the densities $n_\pm(s)$ are very small but nonzero for all s being considered, we can approximate

$$\mu_\pm(s) \approx T \log\left(\frac{n_\pm(s)}{2n_\Lambda}\right), \quad (63)$$

where the log is a large negative number. If we take $|\mu_\pm(s)| \gg 2g_2|\varepsilon(\mathbf{k})|$, equivalent to $T/t \gg 8g_2/|\log(n_\pm(s)/2n_\Lambda)|$, then all frequencies in the integration region are small compared to the chemical potential and we can expand the distribution function in Eq. (62) in powers of ω'. With the factor of ω' already appearing in the integrand the terms at even orders in this expansion integrate identically to zero. The lowest order nonzero term gives

$$\sigma \approx -\frac{4e^2 g_2}{3\pi}\int \mathrm{d}s \int \frac{\mathrm{d}^2k}{(2\pi)^2}\frac{|\boldsymbol{\nabla}_k \varepsilon(\mathbf{k})|^2}{|\varepsilon(\mathbf{k})|}\sum_{\eta=\pm} n'_\eta\left(|\mu_\eta(s)|\right) \approx \frac{2e^2 g_2}{3\pi n_\Lambda T}\int \mathrm{d}s\, n(s) \int \frac{\mathrm{d}^2k}{(2\pi)^2}\frac{|\boldsymbol{\nabla}_k \varepsilon(\mathbf{k})|^2}{|\varepsilon(\mathbf{k})|}, \quad (64)$$

with the higher order terms contributing terms with higher powers in the small constant g_2, and so can be neglected. To reach the final line we used $n_\pm(s) \ll n_\Lambda$ to expand the derivatives of the Bose and Fermi functions and replaced $n_+(s)+n_-(s) = n(s)$. The momentum integral is independent of temperature and can be evaluated expanding $\varepsilon(\mathbf{k})$ around $\mathbf{k}_{0,\pi}$. Dependence on the hole doping p enters through the sum over the cluster numbers, i.e. the critical part of the total density of clusters in the system M_0 as in Eq. (1). (There M_0 is a function of the deviation of the occupation probability from criticality $P - P_c$, but the translation to hole doping $p - p_c$ is trivial.) The resistivity is the inverse of this expression, and so we obtain

$$\rho \sim \frac{T}{M_{0,\mathrm{crit}}(p)}. \quad (65)$$

Though the critical part of M_0 vanishes at the critical point, the finite size of any real system and the non-vanishing contribution from small clusters ensures that the coefficient of this T-linear form does not actually diverge, but nevertheless achieves its largest value at the critical doping p_c—the proliferation of large clusters at the critical point yields the minimum cluster density and maximum resistivity. We also note that the divergent, imaginary Drude term acquires exactly the same dependence on T and p as the real part we have analyzed here explicitly.

Curiously, we have found a linear-in-T resistivity stemming from the Gaussian sector of the model action Eq. (39), which is similar in the form to a random matrix model. The random matrix model has a description in terms of quasiparticles—$g_{\lambda\lambda'}$ can be immediately diagonalized instead of following a Green's function calculation as in Section V B—and therefore is known not to give such anomalous behavior [34]. Here, however, the parameter s and appearance of the momentum-dependent function $\varepsilon(\mathbf{k})$ in the kinetic energy distinguish this model from a random matrix model and allows this result to be obtained. The only energy scales appearing in the spectral densities are the frequency ω and the kinetic energy $g_2|\varepsilon(\mathbf{k})|$, both of which are integrated in order to find the cluster field densities and set the chemical potentials. Thus, in the parameter regime considered the only energy or length scales remaining inside $\mu_\pm(s)$ are the cluster densities $n(s)$ and the temperature. Since s is also integrated, the only scale remaining in the end to determine the behavior of ρ is T.

The approximations made to obtain this result imply that the linear-in-T behavior does not persist down to

$T = 0$ or up to $T \to \infty$, but for a range $g_2 \ll T/t \ll 1$. At this lower limit contributions at higher odd powers of T start to become relevant. We do not have a numerical estimate for the small constant g_2 nor for other factors entering into this lower scale, however, so it is not possible to say precisely at what temperature scale we might expect to see a significant deviation from linear-in-T behavior. Regarding the upper limit, if $t \sim 100\text{meV} \sim 10^3\text{K}$ then we expect non-saturating linear-in-T behavior up to the highest experimentally accessible temperatures.

B. Power-law Optical Conductivity

As found in Section V C, the cubic Green's functions $G_{3,\pm}$ apply over a wide range of frequencies between UV and IR limits for large s. Using these Green's functions in Π we can therefore obtain the leading-order contributions to the optical conductivity relevant in this intermediate frequency regime. A simple scaling analysis of the frequency dependence of this optical conductivity gives

$$\begin{aligned}\sigma(\omega) &= \frac{\Pi(\omega + i0)}{i\omega} \\ &\sim \frac{1}{\omega}\int \mathrm{d}\omega' \sum_{\eta=\pm} G^R_{3,\eta}(\omega') G^A_{3,\eta}(\omega' - \omega) \\ &\sim |\omega|^{-2/3} e^{i\pi/3}. \end{aligned} \quad (66)$$

We therefore find that $\sigma(\omega)$ for this model is of power-law form for a range of intermediate frequencies, with exponent matching the results of experiments in the cuprates [6–11].

To recover power-law behavior here we only need a simple scaling argument using the $T = 0$ form of the cluster Green's functions. In principle, a more precise form for the optical conductivity may be obtained from a more complete analysis, including temperature dependence by extending these Green's functions to non-zero temperature leveraging the cubic regime's imaginary time reparametrization invariance and a conformal transformation, e.g. as discussed in Refs. [28, 31]. We will leave such analysis to later work.

VII. DISCUSSION AND OUTLOOK

The simple first analysis of the transport properties of the model in the previous section yields clear non-Fermi-liquid properties indicative of a strange metal. The optical conductivity has power-law form, $\sigma(\omega) \sim |\omega|^{-2/3}$, and the dc resistivity is found to be linear-in-T with doping-dependent slope that takes its maximum value at the critical doping $p_c \approx 0.1854$, all of which are consistent the phenomenology of the cuprates. Interestingly, these behaviors are found to arise from different sectors of the model. For zero and non-zero frequency different contributions to the self-energies dominate, so although all terms in the model action result from implementing a single principle—a classical percolation transition—particular anomalous properties characteristic of the strange metal phase do not all arise from the same microscopic processes. The dc properties arise from the Gaussian sector of the theory, with the corresponding cluster interaction term related to the shifting of single clusters, while the optical properties arise from the cubic sector, describing the merging and dividing of clusters.

Here we have focused exclusively on $p \leq p_c$ since above this value an infinite cluster appears which requires qualitatively new considerations. However, the model action Eq. (39) does not suddenly become irrelevant above the critical doping. There are still finite clusters for $p > p_c$ that are described by this action, so the contributions to the transport properties that we have calculated will remain, but now in addition to whatever contributions are brought by the infinite cluster. In finite clusters electrons are strictly confined—they may not pass through the large energy barrier at the boundary—but this is not the case for the infinite cluster. In principle electronic wave functions are not forbidden from being extended, though localization may also result from interference effects in any given configuration of the system [68, 69]. However, this quantum percolation problem, as it is called, is somewhat different than what would arises in a percolation-based recasting of the Hubbard model for $p > p_c$, since the infinite cluster itself is not static; the motion of the electrons forming its boundary have dynamics themselves, and further study would be needed to determine how this affects the nature of the electronic states within, i.e. extended, power-law localized, or exponentially localized. Whatever the case, the infinite cluster surely provides a crucial contribution to transport properties above p_c, especially as it grows with higher hole doping to encompass and larger and larger portion of the system. It seems reasonable to guess that this may be related to the emergence of a Fermi-liquid-like state at high enough hole doping.

As noted in the introduction, there are additional properties indicative of the strange metallic phase of the hole-doped cuprates that we have not considered, such as the temperature dependence of Hall properties. Because the construction presented here depends the system possessing spin symmetry while also treating the two electron spins separately—one bounding clusters, the other residing within them—a natural question arises as to how to account for the partial magnetization of the system in response to the external field necessary for Hall response. Our choice here of having spin-down electrons bound clusters was arbitrary, and exchanging spin-up and spin-down everywhere yields the same results. If the system has an excess of one spin species, however, then this symmetry is broken and the doping yielding the percolation transition would shift up or down from the symmetric case depending on the choice. Putting $n_\uparrow = (n_e + \delta)/2$ and $n_\downarrow = (n_e - \delta)/2$, then identifying the critical hole doping as a percolation transition as in

Section III A gives $p_{c\uparrow} \approx 0.1854 + \delta$ and $p_{c\downarrow} \approx 0.1854 - \delta$ depending on whether spin-up or spin-down electrons are taken to bound clusters. If δ is smaller than the uncertainty of the doping level in experiments then this splitting may be irrelevant, and only subsequent effects of an applied magnetic field in our analysis would be necessary to consider. If δ is not small, however, then a qualitatively new calculation is likely required that can manage the split percolation transition for different spins.

The effect of disorder has not been considered here in any real detail. Though we modeled the matrix elements g for the cluster dynamics terms as random quantities, we began from the clean Hubbard Hamiltonian on a perfectly regular square lattice. If, at the level of the Hubbard Hamiltonian, we were to include quenched hopping disorder or an on-site disorder potential characterized by an energy $W \ll U$, then the initial rewriting of the system in terms of clusters is largely unaffected, and our ignoring of rare spatially ordered states would be more explicitly justified. Furthermore, the interaction constants g would be affected by either of these forms of disorder to become actually random quantities.

Another question we have not fully addressed here is the range of temperatures for which this theory applies, or how other phases emerge from this state and dominate at low temperatures. In the cuprates, for $p < p_c$ strange metallic behavior gives way to the pseudogap phase below a crossover temperature T^* that decreases with increasing hole doping and drops to 0 at $p = p_c$. Since it vanishes at p_c, can we understand T^* as related to some critical behavior of the percolation transition? The correlation length characterizing the largest cluster ξ provides one natural IR cutoff for the theory, $E_\xi \sim 1/\xi \sim |p - p_c|^{\nu_P}$, which decreases with increasing p and vanishes at the critical point. On length scales larger than ξ or energy scales smaller than E_ξ the cluster structure cannot be distinguished and the theory investigated here is invalid, which may signal one avenue to approach the emergence of new phases at low temperatures.

Most notably superconductivity arises in the cuprates in a low-temperature dome covering a range of dopings around p_c. The model proposed here does not possess a mechanism for forming Cooper pairs, though the analysis has not considered the spin-spin interaction, parameterized by $J \sim t^2/U$, generated by virtual double-occupancy. This interaction favors the formation spin singlet states on nearest neighbor sites, which in the cluster picture may occur at the boundaries of the clusters—spin-down electrons bound the clusters filled with spin-up electrons. Therefore we see that the sorts of clusters we have been considering, which have fractal properties on average and large surface areas, are energetically favored by including this additional term in the Hamiltonian compared to, for example, clusters with more circular geometry. Additionally, when $T \sim J$ the pairing effect of the spin-spin interaction will become important and may dominate, causing the principle assumptions of this work to fail. It is currently unclear how to include all effects of this J interaction into the model action Eq. (39) and therefore we cannot yet explore how superconductivity may emerge at low temperatures.

The goal of this work is to attempt to bridge the gap between the Hubbard model, a well accepted starting point for the analysis of real strongly-correlated system, especially the cuprate high-temperature superconductors, and theories yielding strange-metallic properties, which often lack a clear connection to the microscopic physics of electrons in a lattice. We have shown that rewriting the infinite-U Hubbard model in a way that highlights the classical percolation transition occurring in the basis states at hole doping $p_c \approx 0.1854$ motivates a model that exhibits strange-metallic behavior, and has features of a number of different types of theories: it is a large-N model like SYK and its relatives and the cluster size s plays a similar role to the continuous mass spectrum in theories of unparticles. The degrees of freedom of this theory originate from extended clusters of electrons in the original real-space electronic basis, and the large number of "flavors" in the model are related to the large number of possible shapes for clusters of sufficient size, which are responsible for the critical properties of the percolation transition itself. Ultimately, the strange metallic transport of the model is due the scaling properties of these degrees of freedom and the unusual nature of their dynamics.

Though we have not provided a rigorous derivation of the effective theory Eq. (39) from the Hubbard model, the ability of the model to recover the transport properties in line with experiments in the cuprates without fine tuning or *ad hoc* additional degrees of freedom and to naturally explain why these properties manifest near $p \sim 0.19$ specifically, suggests that this framework may be relevant for understanding the nature of the cuprate normal state. There is much more to be studied about this model, both at the level of the microscopic construction in Sections III and IV and in the model action in Section V, most importantly the potential to support superconductivity and other low-temperature phases by including additional perturbations.

ACKNOWLEDGMENTS

I would like to thank Nigel Cooper, Pieter Claeys, Jan Behrends, Justin Wilson, Zachary Raines, Daniel Sheehy, Ilya Vekhter, Haoyu Guo, and Elio König for helpful discussions. This work was performed in part at the Aspen Center for Physics, which is supported by the National Science Foundation Grant No. PHY-1607611.

Appendix A: Boundary electron hopping matrix elements

Here we give an explicit calculation for a general matrix element for the spin-down hopping term in the cluster

basis. In the initial set of clusters $\mathscr{C}$, there are N_c clusters that have a particular spin-down electron forming part of their boundary, and when this electron hops we are taken to a different set of clusters $\mathscr{C}'$ in which those initial clusters have been changed into N_c' new clusters. We label the initial clusters $\zeta_1, \ldots, \zeta_{N_c}$ and the final clusters $\zeta_1', \ldots, \zeta_{N_c'}'$. We define the union of the sites in the initial and final sets of clusters respectively as Z_c and Z_c'. Since the total number of spin-up electrons within the initial and final clusters cannot change we have

$$\nu = \sum_{i=1}^{N_c} \nu_i = \sum_{j=1}^{N_c'} \nu_j' = \nu', \tag{A1}$$

and similarly the total number of sites in the initial and final sets of clusters cannot change, so we have

$$s = \sum_{i=1}^{N_c} s_i = \sum_{j=1}^{N_c'} s_j' = s'. \tag{A2}$$

We also know how the total center of mass of the involved clusters moves; the sets Z_c and Z_c' differ in the location of a single site, which is displaced by $-\hat{\mathbf{e}}$, so the the total final center of mass $\mathbf{r}'$ is related to the total initial center of mass $\mathbf{r}$ via

$$\mathbf{r}' = \mathbf{r} - \frac{\hat{\mathbf{e}}}{s}. \tag{A3}$$

Finally we introduce the abbreviated notation $\alpha_i = \zeta_i, \hat{\nu}_i = \mathbf{r}_i, s_i, \lambda_i, \mathcal{I}_i$. With this notation in place we can write the spin-down electron hopping matrix element in the cluster basis as

$$\begin{aligned}
\langle \{\mathcal{I}'\}, \mathscr{C}' | \left(-t \sum_{\hat{\mathbf{e}}} c^\dagger_{\mathbf{x}+\hat{\mathbf{e}},\downarrow} c_{\mathbf{x},\downarrow} \right) | \{\mathcal{I}\}, \mathscr{C} \rangle &= -t \bigoplus_{i=1}^{N_c'} \bigoplus_{j=1}^{N_c} \langle \varnothing, \zeta_i' | \, C_{\alpha_i'} \sum_{\hat{\mathbf{e}}} c^\dagger_{\mathbf{x}+\hat{\mathbf{e}},\downarrow} c_{\mathbf{x},\downarrow} C^\dagger_{\alpha_j} \, | \varnothing, \zeta_j \rangle \\
= -t \bigoplus_{i=1}^{N_c'} \bigoplus_{j=1}^{N_c} \langle \varnothing, \zeta_i' | \sum_{\{\mathbf{x}_i\} \in \zeta_i'} c_{\mathbf{x}_{i,1}} \cdots c_{\mathbf{x}_{i,\nu_i'}} \Phi^*_{\alpha_i'}(\mathbf{x}_{i,1}, \ldots, \mathbf{x}_{i,\nu_i'}) \sum_{\hat{\mathbf{e}}} c^\dagger_{\mathbf{x}+\hat{\mathbf{e}},\downarrow} c_{\mathbf{x},\downarrow} \sum_{\{\mathbf{y}_j\} \in \zeta_j} \Phi_{\alpha_j}(\mathbf{y}_{j,1}, \ldots, \mathbf{y}_{j,\nu_j}) c^\dagger_{\mathbf{y}_{j,\nu_j}} \cdots c^\dagger_{\mathbf{y}_{j,1}} \, | \varnothing, \zeta_j \rangle \\
= -t \, \delta_{\nu',\nu} \delta_{s',s} \delta_{\mathbf{r}',\mathbf{r}-\hat{\mathbf{e}}/s} \sum_{\{\mathbf{x}\} \in Z_c'} \Phi^*_{\alpha_1' \ldots \alpha_{N_c'}'}(\mathbf{x}_1, \ldots, \mathbf{x}_{\nu'}) \Phi_{\alpha_1 \ldots \alpha_{N_c}}(\mathbf{x}_1, \ldots, \mathbf{x}_\nu) \\
\equiv -t \, g^{(N_c \to N_c')}_{\alpha_1' \ldots \alpha_{N_c'}'; \alpha_1 \ldots \alpha_{N_c}}.
\end{aligned} \tag{A4}$$

In the third line we define the multi-cluster, multi-electron wave functions as the product of the multi-electron wave functions in the clusters in question,

$$\Phi_{\alpha_1 \ldots \alpha_N}(\mathbf{x}_1, \ldots, \mathbf{x}_\nu) = \Phi_{\alpha_1}(\mathbf{x}_1, \ldots, \mathbf{x}_{\nu_1}) \cdots \Phi_{\alpha_N}(\mathbf{x}_{\nu - \nu_N + 1}, \ldots, \mathbf{x}_{\nu_N}), \tag{A5}$$

and in the final line we define the symbol $g^{(N_c \to N_c')}_{\alpha_1' \ldots \alpha_{N_c'}'; \alpha_1 \ldots \alpha_{N_c}}$ to represent the entire inner product of the initial and final multi-electron wave functions, including the δ-functions enforcing conservation of electron number and total cluster size, and the motion of the cluster center of mass.

Appendix B: Internal spectra of large clusters

Here we investigate the question of how well the single-particle spectra within individual large clusters are approximated by the average over cluster shapes. We examine this question numerically: for a range of different sizes we generate a large number of random clusters, obtaining a representative sample of the vast number of cluster shapes, then diagonalize the nearest-neighbor hopping Hamiltonian and average the energies thus obtained. The discrete indices labeling these averaged energies, $i = 1, 2, \ldots, s$ are then related to samplings of a continuous parameter x running from 0 to 1 as $x_i = i/(s+1)$. The result of this procedure for $s = 50, 75, 100$, and 200, averaging over 100 different shapes each, is shown in Fig. 7. The average spectra for different sized clusters are found to trace the same curve as a function of the parameter x, and we define this function to be the continuous spectrum $\bar{\epsilon}(x)$.

Appendix C: Evaluation of scaling Green's functions, G_3

Here we determine the values of the exponents $\gamma_\pm$ and $\Delta_\pm$ and the behavior of the functions $\Omega_\pm(\mathbf{k})$ and $\theta_\pm(s)$

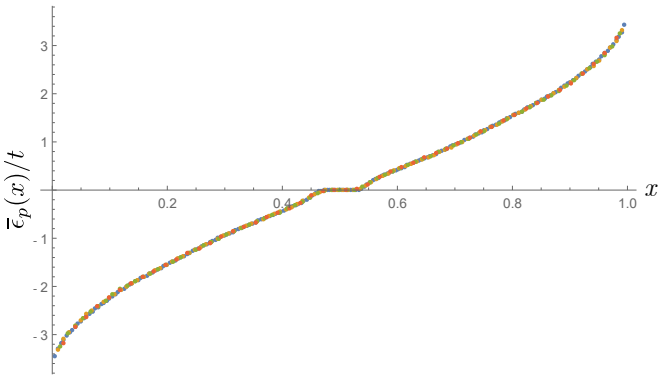

FIG. 7. The average spectra for clusters of size 50 (red), 75 (green), 100 (yellow), and 200 (blue). For each size we generate 100 random clusters, find and sort the energies of the s eigenstates, then average each energy in order. The horizontal axis is the index of the state over $s+1$. We see that they all follow the same curve which we call $\bar{\epsilon}_p(x)$, with the average energies for a cluster of size s very closely reproduced as the values of $\bar{\epsilon}_p(x)$ at the points $x_i = i/(s+1)$ for $i = 1, 2, \ldots, s$.

appearing in the scaling ansatz for the Green's function in the cubic regime, $G_{3,\pm}$. To do so we employ the spectral representation of the Green's function for complex frequency z,

$$G_{3,\pm}(z, \mathbf{k}, s) = \int_{-\infty}^{\infty} \mathrm{d}\omega \frac{\rho_{3,\pm}(\omega, \mathbf{k}, s)}{z - \omega}, \tag{C1}$$

and impose the appropriate positivity constraints on the spectral density for bosons and fermions, $-\operatorname{Im} G_{3,-}(\omega + i0) > 0$ and $-\omega \operatorname{Im} G_{3,+}(\omega + i0) > 0$. These immediately give

$$-\pi\Delta_- < \theta_-(s) < \pi\Delta_- \tag{C2}$$

$$\pi\Delta_+ < \theta_+(s) < \pi(1 - \Delta_+). \tag{C3}$$

Fourier transforming the spectral representation of $G_{3,\pm}$ to imaginary time τ we have

$$G_{3,\pm}(\tau, \mathbf{k}, s) = \begin{cases} -\int_0^\infty \mathrm{d}\omega \rho_{3,\pm}(\omega, \mathbf{k}, s) e^{-\omega\tau}, & \tau > 0 \\ \int_0^\infty \mathrm{d}\omega \rho_{3,\pm}(-\omega, \mathbf{k}, s) e^{-\omega|\tau|}, & \tau < 0, \end{cases} \tag{C4}$$

with which we can write the imaginary time representation of the Green's functions,

$$G_{3,\pm}(\tau, \mathbf{k}, s) = -\operatorname{sgn}(\tau) \frac{s^{\gamma_\pm} \Gamma(2\Delta_\pm)}{\pi \Omega_\pm(\mathbf{k})^{2\Delta_\pm} |\tau|^{2\Delta_\pm}} \times \sin\left(\pi\Delta_\pm + \operatorname{sgn}(\tau)\theta_\pm(s)\right). \tag{C5}$$

Substituting this into Eqs. (42) and (43), the cubic terms of the self-energies, which we denote $\Sigma_{3,\pm}(\tau, \mathbf{k}, s)$, can then be written explicitly.

Alternatively, we can start from the Dyson equation,

$$G_{3,\pm}(z, \mathbf{k}, s)^{-1} = z + \mu_\pm(s) - \Sigma_{3,\pm}(z, \mathbf{k}, s). \tag{C6}$$

If we assume that the zero-frequency part of the self-energy cancels the chemical potential, then for $z \neq 0$ we have

$$\Sigma_{3,\pm}(z, \mathbf{k}, s) = z - s^{-\gamma_\pm} \Omega_\pm(\mathbf{k})^{2\Delta_\pm} e^{i(\pi\Delta_\pm + \theta_\pm(s))} z^{1-2\Delta_\pm}. \tag{C7}$$

Using a spectral representation for Σ in terms of a function σ (as G is written in terms of ρ) and a Fourier transform of this spectral representation we obtain a second expression for the self-energies in terms of the imaginary time τ,

$$\Sigma_{3,\pm}(\tau, \mathbf{k}, s) = -\operatorname{sgn}(\tau) s^{-\gamma_\pm} \frac{\Gamma(2 - 2\Delta_\pm)}{\pi |\tau|^{2-2\Delta_\pm}} \Omega_\pm(\mathbf{k})^{2\Delta_\pm} \times \sin\left(\pi\Delta_\pm + \operatorname{sgn}(\tau)\theta_\pm(s)\right). \tag{C8}$$

Equating the two representations we have thus obtained for $\Sigma_{3,\pm}(\tau, \mathbf{k}, s)$ and demanding consistency for generic s and in the limit $s \to s_\xi$ gives $\Delta_\pm = 1/3$ and $\gamma_\pm = -1/3$, and also constrains $\Omega_\pm(\mathbf{k}) \propto \varepsilon(\mathbf{k})$.

[1] R. J. Cava, B. Batlogg, R. B. van Dover, D. W. Murphy, S. Sunshine, T. Siegrist, J. P. Remeika, E. A. Rietman, S. Zahurak, and G. P. Espinosa, Bulk superconductivity at 91 K in single-phase oxygen-deficient perovskite $Ba_2YCu_3O_{9-\delta}$, Phys. Rev. Lett. **58**, 1676 (1987).

[2] M. Gurvitch and A. T. Fiory, Resistivity of $La_{1.825}Sr_{0.175}CuO_4$ and $YBa_2Cu_3O_7$ to 1100 K: Absence of saturation and its implications, Phys. Rev. Lett. **59**, 1337 (1987).

[3] T. Manako, Y. Kubo, and Y. Shimakawa, Transport and structural study of $Tl_2Ba_2CuO_{6+\delta}$ single crystals prepared by the KCl flux method, Phys. Rev. B **46**, 11019 (1992).

[4] S. Nakamae, K. Behnia, N. Mangkorntong, M. Nohara, H. Takagi, S. J. C. Yates, and N. E. Hussey, Electronic ground state of heavily overdoped nonsuperconducting $La_{2-x}Sr_xCuO_4$, Phys. Rev. B **68**, 100502 (2003).

[5] R. A. Cooper, Y. Wang, B. Vignolle, O. J. Lipscombe, S. M. Hayden, Y. Tanabe, T. Adachi, Y. Koike, M. Nohara, H. Takagi, C. Proust, and N. E. Hussey, Anomalous Criticality in the Electrical Resistivity of $La_{2-x}Sr_xCuO_4$, Science **323**, 603 (2009), https://www.science.org/doi/pdf/10.1126/science.1165015.

[6] S. L. Cooper, G. A. Thomas, J. Orenstein, D. H. Rapkine, A. J. Millis, S.-W. Cheong, A. S. Cooper, and Z. Fisk, Growth of the optical conductivity in the Cu-O planes, Phys. Rev. B **41**, 11605 (1990).

[7] Z. Schlesinger, R. T. Collins, F. Holtzberg, C. Feild, S. H. Blanton, U. Welp, G. W. Crabtree, Y. Fang, and J. Z. Liu, Superconducting energy gap and normal-state conductivity of a single-domain $YBa_2Cu_3O_7$ crystal, Phys. Rev. Lett. **65**, 801 (1990).

[8] A. El Azrak, R. Nahoum, N. Bontemps, M. Guilloux-Viry, C. Thivet, A. Perrin, S. Labdi, Z. Z. Li, and H. Raffy, Infrared properties of $YBa_2Cu_3O_7$ and $Bi_2Sr_2Ca_{n-1}Cu_nO_{2n+4}$ thin films, Phys. Rev. B **49**, 9846 (1994).

[9] C. Baraduc, A. El Azrak, and N. Bontemps, Infrared conductivity in the normal state of cuprate thin films, Journal of Superconductivity **9**, 3 (1996).

[10] D. v. d. Marel, H. J. A. Molegraaf, J. Zaanen, Z. Nussinov, F. Carbone, A. Damascelli, H. Eisaki, M. Greven, P. H. Kes, and M. Li, Quantum critical behaviour in a high-T_c superconductor, Nature **425**, 271 (2003).

[11] J. Hwang, T. Timusk, and G. D. Gu, Doping dependent optical properties of $Bi_2Sr_2CaCu_2O_{8+\delta}$, Journal of Physics: Condensed Matter **19**, 125208 (2007).

[12] T. R. Chien, D. A. Brawner, Z. Z. Wang, and N. P. Ong, Unusual $1/T^3$ temperature dependence of the Hall conductivity in $YBa_2Cu_3O_{7-\delta}$, Phys. Rev. B **43**, 6242 (1991).

[13] A. Carrington, D. J. C. Walker, A. P. Mackenzie, and J. R. Cooper, Hall effect and resistivity of oxygen-deficient $YBa_2Cu_3O_{7-\delta}$ thin films, Phys. Rev. B **48**, 13051 (1993).

[14] K. Segawa and Y. Ando, Intrinsic Hall response of the CuO_2 planes in a chain-plane composite system of $YBa_2Cu_3O_y$, Phys. Rev. B **69**, 104521 (2004).

[15] S.-D. Chen, M. Hashimoto, Y. He, D. Song, K.-J. Xu, J.-F. He, T. P. Devereaux, H. Eisaki, D.-H. Lu, J. Zaanen, and Z.-X. Shen, Incoherent strange metal sharply bounded by a critical doping in Bi2212, Science **366**, 1099 (2019), https://www.science.org/doi/pdf/10.1126/science.aaw8850.

[16] E. Dagotto, Correlated electrons in high-temperature superconductors, Rev. Mod. Phys. **66**, 763 (1994).

[17] M. Imada, A. Fujimori, and Y. Tokura, Metal-insulator transitions, Rev. Mod. Phys. **70**, 1039 (1998).

[18] C. M. Varma, P. B. Littlewood, S. Schmitt-Rink, E. Abrahams, and A. E. Ruckenstein, Phenomenology of the normal state of Cu-O high-temperature superconductors, Phys. Rev. Lett. **63**, 1996 (1989).

[19] Y. Kakehashi and P. Fulde, Marginal Fermi Liquid Theory in the Hubbard Model, Phys. Rev. Lett. **94**, 156401 (2005).

[20] N. S. Vidhyadhiraja, A. Macridin, C. Şen, M. Jarrell, and M. Ma, Quantum Critical Point at Finite Doping in the 2D Hubbard Model: A Dynamical Cluster Quantum Monte Carlo Study, Phys. Rev. Lett. **102**, 206407 (2009).

[21] E. W. Huang, R. Sheppard, B. Moritz, and T. P. Devereaux, Strange metallicity in the doped Hubbard model, Science **366**, 987 (2019), https://www.science.org/doi/pdf/10.1126/science.aau7063.

[22] W. Wú, X. Wang, and A.-M. Tremblay, Non-Fermi liquid phase and linear-in-temperature scattering rate in overdoped two-dimensional Hubbard model, Proceedings of the National Academy of Sciences **119**, e2115819119 (2022), https://www.pnas.org/doi/pdf/10.1073/pnas.2115819119.

[23] E. Perepelitsky, A. Galatas, J. Mravlje, R. Žitko, E. Khatami, B. S. Shastry, and A. Georges, Transport and optical conductivity in the Hubbard model: A high-temperature expansion perspective, Phys. Rev. B **94**, 235115 (2016).

[24] W. Xu, W. McGehee, W. Morong, and B. DeMarco, Bad-Metal Relaxation Dynamics in a Fermi Lattice Gas (2018), arXiv:1606.06669 [cond-mat.quant-gas].

[25] P. T. Brown, D. Mitra, E. Guardado-Sanchez, R. Nourafkan, A. Reymbaut, C.-D. Hébert, S. Bergeron, A.-M. S. Tremblay, J. Kokalj, D. A. Huse, P. Schauß, and W. S. Bakr, Bad metallic transport in a cold atom Fermi-Hubbard system, Science **363**, 379 (2019), https://www.science.org/doi/pdf/10.1126/science.aat4134.

[26] S. Sachdev and J. Ye, Gapless spin-fluid ground state in a random quantum Heisenberg magnet, Phys. Rev. Lett. **70**, 3339 (1993).

[27] O. Parcollet, A. Georges, G. Kotliar, and A. Sengupta, Overscreened multichannel SU(N) Kondo model: Large-N solution and conformal field theory, Phys. Rev. B **58**, 3794 (1998).

[28] O. Parcollet and A. Georges, Non-Fermi-liquid regime of a doped Mott insulator, Phys. Rev. B **59**, 5341 (1999).

[29] A. Kitaev, A simple model of quantum holography (part 1) (2015), talk at KITP.

[30] A. Kitaev, A simple model of quantum holography (part 2) (2015), talk at KITP.

[31] S. Sachdev, Bekenstein-Hawking Entropy and Strange Metals, Phys. Rev. X **5**, 041025 (2015).

[32] I. Esterlis and J. Schmalian, Cooper pairing of incoherent electrons: An electron-phonon version of the Sachdev-Ye-Kitaev model, Phys. Rev. B **100**, 115132 (2019).

[33] D. Chowdhury, A. Georges, O. Parcollet, and S. Sachdev, Sachdev-Ye-Kitaev models and beyond: Window into non-Fermi liquids, Rev. Mod. Phys. **94**, 035004 (2022).

[34] S. Sachdev, *Quantum Phases of Matter* (Cambridge University Press, 2023).

[35] S. A. Hartnoll, A. Lucas, and S. Sachdev, *Holographic Quantum Matter* (The MIT Press, 2018).

[36] P. Coleman, C. Pépin, Q. Si, and R. Ramazashvili, How do Fermi liquids get heavy and die?, Journal of Physics: Condensed Matter **13**, R723 (2001).

[37] S. Florens and A. Georges, Slave-rotor mean-field theories of strongly correlated systems and the Mott transition in finite dimensions, Phys. Rev. B **70**, 035114 (2004).

[38] T. Senthil, Critical Fermi surfaces and non-Fermi liquid metals, Phys. Rev. B **78**, 035103 (2008).

[39] T. Senthil, Theory of a continuous Mott transition in two dimensions, Phys. Rev. B **78**, 045109 (2008).

[40] H. Georgi, Unparticle Physics, Phys. Rev. Lett. **98**, 221601 (2007).

[41] P. W. Phillips, B. W. Langley, and J. A. Hutasoit, Un-Fermi liquids: Unparticles in strongly correlated electron matter, Phys. Rev. B **88**, 115129 (2013).

[42] A. Karch, K. Limtragool, and P. W. Phillips, Unparticles and anomalous dimensions in the cuprates, Journal of High Energy Physics **2016**, 175 (2016).

[43] K. Limtragool, C. Setty, Z. Leong, and P. W. Phillips, Realizing infrared power-law liquids in the cuprates from unparticle interactions, Phys. Rev. B **94**, 235121 (2016).

[44] Z. Leong, C. Setty, K. Limtragool, and P. W. Phillips, Power-law liquid in cuprate superconductors from fermionic unparticles, Phys. Rev. B **96**, 205101 (2017).

[45] A. V. Andreev, S. A. Kivelson, and B. Spivak, Hydrodynamic description of transport in strongly correlated electron systems, Phys. Rev. Lett. **106**, 256804 (2011).

[46] S. A. Hartnoll, Theory of universal incoherent metallic transport, Nature Physics **11**, 54 (2015).

[47] A. Lucas, Hydrodynamic transport in strongly coupled disordered quantum field theories, New Journal of Physics **17**, 113007 (2015).

[48] A. Lucas, J. Crossno, K. C. Fong, P. Kim, and S. Sachdev, Transport in inhomogeneous quantum critical fluids and in the Dirac fluid in graphene, Phys. Rev. B **93**, 075426 (2016).

[49] A. Lucas and S. A. Hartnoll, Resistivity bound for hydrodynamic bad metals, Proceedings of the National Academy of Sciences **114**, 11344 (2017), https://www.pnas.org/doi/pdf/10.1073/pnas.1711414114.

[50] A. Aharony and D. Stauffer, *Introduction To Percolation Theory* (Taylor & Francis, 2003).

[51] D. Stauffer, Scaling theory of percolation clusters, Physics Reports **54**, 1 (1979).

[52] We use the subscript P to unambiguously specify quantities associated with the percolation transition.

[53] M. C. Gutzwiller, Correlation of electrons in a narrow s band, Phys. Rev. **137**, A1726 (1965).

[54] J. Loram, J. Luo, J. Cooper, W. Liang, and J. Tallon, Evidence on the pseudogap and condensate from the electronic specific heat, Journal of Physics and Chemistry of Solids **62**, 59 (2001).

[55] J. Tallon and J. Loram, The doping dependence of T* – what is the real high-Tc phase diagram?, Physica C: Superconductivity **349**, 53 (2001).

[56] J. L. Tallon, J. G. Storey, J. R. Cooper, and J. W. Loram, Locating the pseudogap closing point in cuprate superconductors: Absence of entrant or reentrant behavior, Phys. Rev. B **101**, 174512 (2020).

[57] C. Proust and L. Taillefer, The remarkable underlying ground states of cuprate superconductors, Annual Review of Condensed Matter Physics **10**, 409 (2019), https://doi.org/10.1146/annurev-conmatphys-031218-013210.

[58] C. E. Matt, C. G. Fatuzzo, Y. Sassa, M. Månsson, S. Fatale, V. Bitetta, X. Shi, S. Pailhès, M. H. Berntsen, T. Kurosawa, M. Oda, N. Momono, O. J. Lipscombe, S. M. Hayden, J.-Q. Yan, J.-S. Zhou, J. B. Goodenough, S. Pyon, T. Takayama, H. Takagi, L. Patthey, A. Bendounan, E. Razzoli, M. Shi, N. C. Plumb, M. Radovic, M. Grioni, J. Mesot, O. Tjernberg, and J. Chang, Electron scattering, charge order, and pseudogap physics in $La_{1.6-x}Nd_{0.4}Sr_xCuO_4$: An angle-resolved photoemission spectroscopy study, Phys. Rev. B **92**, 134524 (2015).

[59] C. Collignon, S. Badoux, S. A. A. Afshar, B. Michon, F. Laliberté, O. Cyr-Choinière, J.-S. Zhou, S. Licciardello, S. Wiedmann, N. Doiron-Leyraud, and L. Taillefer, Fermi-surface transformation across the pseudogap critical point of the cuprate superconductor $la_{1.6-x}nd_{0.4}sr_xcuo_4$, Phys. Rev. B **95**, 224517 (2017).

[60] C. Fortuin and P. Kasteleyn, On the random-cluster model: I. introduction and relation to other models, Physica **57**, 536 (1972).

[61] G. Grimmett, The random-cluster model (2003), arXiv:math/0205237 [math.PR].

[62] D. Redelmeier, Counting polyominoes: Yet another attack, Discrete Mathematics **36**, 191 (1981).

[63] X. R. Wang, Localization in fractal spaces: Exact results on the sierpinski gasket, Phys. Rev. B **51**, 9310 (1995).

[64] E. J. König, P. M. Ostrovsky, I. V. Protopopov, and A. D. Mirlin, Metal-insulator transition in two-dimensional random fermion systems of chiral symmetry classes, Phys. Rev. B **85**, 195130 (2012).

[65] E. van Veen, S. Yuan, M. I. Katsnelson, M. Polini, and A. Tomadin, Quantum transport in sierpinski carpets, Phys. Rev. B **93**, 115428 (2016).

[66] S. N. Kempkes, M. R. Slot, S. E. Freeney, S. J. M. Zevenhuizen, D. Vanmaekelbergh, I. Swart, and C. M. Smith, Design and characterization of electrons in a fractal geometry, Nature Physics **15**, 127 (2019).

[67] Y. Gu, A. Kitaev, S. Sachdev, and G. Tarnopolsky, Notes on the complex Sachdev-Ye-Kitaev model, Journal of High Energy Physics **2020**, 157 (2020).

[68] A. Mookerjee, I. Dasgupta, and T. Saha, Quantum Percolation, Int. J. Mod. Phys. B **09**, 2989 (1995).

[69] P. M. Ostrovsky, I. V. Protopopov, E. J. König, I. V. Gornyi, A. D. Mirlin, and M. A. Skvortsov, Density of States in a Two-Dimensional Chiral Metal with Vacancies, Phys. Rev. Lett. **113**, 186803 (2014).